Bulletin of Engineering Geology and the Environment (2025) 84:223
https://doi.org/10.1007/s10064-025-04224-z

ORIGINAL PAPER

Weathering profile of completely weathered rock from the Dullstroom Formation, South Africa

Duan Swart[1,2] · **Matthys A. Dippenaar**[1]

Received: 9 July 2024 / Accepted: 17 March 2025

Abstract
This study investigates the weathering profile of completely weathered rock derived from the Dullstroom Formation in South Africa. The research emphasizes the significance of the soil-rock interface, particularly the transition between completely weathered rock and residual soil, in understanding mechanical, chemical, and hydraulic behaviours. Field sampling and laboratory analyses, including particle size distribution, Atterberg limits, X-ray fluorescence (XRF), X-ray diffraction (XRD), and X-ray Computed Tomography (XRCT), were conducted. XRCT proved invaluable in visualizing pore geometry, density contrasts, and the persistence of relict rock structures in three dimensions. The findings highlight how structural *prominence* decreases with increasing weathering intensity, influencing compressibility and porosity. The compressibility of the material correlates better with chemical weathering indices than traditional geotechnical parameters like void ratio or dry density. These insights contribute to the geotechnical characterization of weathered rock profiles and propose structural *prominence* as a novel parameter for evaluating mechanical behaviour across weathering stages.

Keywords Porosity · XRCT scan · Relict rock structure · Weathering profile · Structural prominence

Introduction

Overview

Weathering rock profiles are frequently encountered during geological, engineering, hydrological, ecological and forestry projects in South Africa. The soil-rock interface typically exists in the most decomposed portion of a weathering rock profile. This interface comprises residual soil and completely weathered rock, both of which can be excavated as a soil. The term saprolite is often used to collectively define this portion of a weathering profile (National Research 2001; Dos Santos et al. 2018; Dos Santos et al. 2022a, b; Silva et al. 2022; Bonnet et al. 2022). To keep to international standards in geotechnics and geology the definitions of residual soil and completely weathered rock will be used in place of the saprolite (ISRM 1981; Dippenaar et al. 2024). ISRM (1981) defines these two weathering states as follows:

- Completely weathered rock: "All rock material is decomposed and/or disintegrated to soil. The original mass structure is still largely intact."
- Residual soil: "All rock material is converted to soil. The mass structure and material fabric are destroyed. There is a large change in volume, but the soil has not been significantly transported."

Dippenaar et al. (2024) defines the completely weathered rock with the same diagnostic features as the above ISRM (1981) definition. The residual soil definition is slightly different and stated as follows by Dippenaar et al. (2024):

- Residual soil: "Rock weathered to the state where original minerals, structures and textures have been altered or removed by weathering."

The boundary between the completely weathered rock and residual soil is defined first by the loss in relict rock structure. Relict rock structure refers to the preserved

✉ Matthys A. Dippenaar
madippenaar@gmail.com

[1] Geology Department, University of Pretoria, Hatfield 0028, South Africa

[2] PeraGage, South Africa

Published online: 10 April 2025

structural features of the original parent rock that remain intact within completely weathered rock, even though the material has undergone significant decomposition and transformation. These features include mineral grains, fractures, joints, foliation, or other textural and structural characteristics inherited from the parent rock. Secondly, a significant change in chemical mineralogy forms in conjunction with an alteration physical state. The decompositions of most to all primary rock forming minerals to secondary minerals, the increase in pedogenic iron oxides and aluminium, and relative increase in silica results in the formation of a residual soil.

Pedogenic oxides are typically iron and aluminium rich secondary minerals formed during soil and weathering processes under the influence of pedogenesis. In rock, the material forms in joints and fractures where water flow occurs.

The formation of these two horizons is dependent on parent material, rainfall, temperature / radiation, evaporation, vegetation cover, time, and topography, with different intensities of each resulting in different profiles and geotechnical conditions. This section will discuss the formation of completely weathered rock and residual soil, which will collectively be called residuum, in a humid climate and will elucidate the alterations the material goes through both from a chemical and structural aspect (Bonnet et al. 2022).

Completely weathered rock's ability to store water influences groundwater recharge and return flow, which affects both the quantity and quality of surface and subsurface waters (National Research 2001; van Tol 2020Dippenaar et al. 2022). In this material, the porosity is a combination of primary voids between mineral grains and secondary fractures inherited from the original rock structure. These secondary pores often serve as preferential flow paths for moisture until the relict rock structure is completely loss through further decomposition, contributing to the complex hydrological behaviour of weathered profiles (Dos Santos et al. 2018; Swart et al. 2019; Jaques et al. 2020; Dos Santos et al. 2022a, b; Bonnet et al. 2022).

Completely weathered rock exposed in large manmade excavations undergo rapid weathering, decomposing metastable minerals, and ultimately alters or destroys the relict rock structure (Obermeier and Langer 1986). It is clear the relict rock structure and fabric is highly dependent on the chemical weathering intensity it is exposed to, and therefore the parameters that this structure governs is influenced by the weathering.

Pore geometry and orientation, governed by relict rock structure, critically influence material strength (Day 1981; Buttrick 1986; Letey 1991; Rocchi et al. 2017; Rabot et al. 2018; Swart et al. 2019; Silva et al. 2022; Dos Santos et al. 2022a, b; Bonnet et al. 2023; Wang et al. 2024). The relict rock structure is thought to provide strength and stiff to completely weathered rock, however it cannot accurately be assessed using standard microscopy methods and hand samples. These methods characterise the structure in 2-dimensions and the structure needs to be broken to being the evaluation.

Pores have been defined as *the sine qua non of soil* (Clothier 2008), in other words, the intrinsic characteristic which soil cannot be without. Pores are open spaces of the soil that are not occupied by solid grains. The porosity of a soil is distributed across a wide range of pore sizes and shapes, ranging from spaces between clay platelets to large open root or burrow channels. Dippenaar (2014) conducted a detailed review of porosity present in both soil and rock and how these are defined and quantified across multi-disciplinary applications. A fundamental concept in hydrology needs to be highlighted, namely the connectivity of porosity. Two types of pores exist in soil, non-effective porosity meaning there is no contribution to the movement of gas or liquids, and effective porosity which are drainable pores and governs the hydraulic conductivity.

Residual soils and completely weathered rock are often associated with tropical climates where intense leaching occurs. *Tropical* soils are not normally associated with South Africa but due to the ancient and stable landscape, deeply weathered rock profiles do exist and are currently forming in the eastern parts of the country. The impact of chemical weathering on the mechanical, chemical and physical parameters has been intensely studied on igneous weathering profiles in high rainfall areas around the world. However, very little work has been done of investigating the influence of decomposition on mechanical and hydraulic properties through a weathered rock profile in South Africa, especially in the past decade (Van der Merwe 1964; Blight and Leong 2012).

The *soil-end* of a weathering profile comprising completely weathered rock and residual soil is the most intricate portion of the profile. It is encountered the most often in geotechnical projects due to it being the closest to the ground surface and furthest away from the weathering front. The properties that seem to be influenced by the completely weathered rock are the parent rock origin and stress history and the weathering state of the completely weathered rock.

By investigating the aims thoroughly, the study seeks to contribute to a better understanding of the engineering characteristics of a weathered rock profile and the soil-rock interface, and how this evolves through further decomposition and anthropogenic interactions. Furthermore, test the usability of x-ray scanning to be used to assess extremely weak rock and residual soil which is too friable to be tested using conventional rock testing methodologies, such as thin sections.

Parent rock decomposition

The residuum forms by weathering via physical, chemical and biological processes (Blight and Leong 2012). Physical processes mechanically disintegrate rock that will expose fresh rock to chemical weathering, increase permeability and surface area of bedrock to allow flow and increased interaction with chemically active fluid. Chemical weathering alters rock minerals through hydration, hydrolysis, carbonation, dissolution, cation exchange and oxidation, forming clay minerals with lower energy states that are more stable (Mitchell and Soga 2005; Yong 2012; Summerfield 2014; Liu et al. 2022; Cho and Ohta 2022; Sergeev 2023).

Rock minerals are not equally susceptible to chemical breakdown and mineralogic change. Typically, the minerals that form at the highest temperature, meaning the first minerals to form during cooling of magma and forming igneous rocks, are the least stable at low temperature at ground surface (Bowen 1929; Goldich 1938). The resultant secondary minerals present in the completely weathered rock and residual soils are further influenced by the intensity to which the weathering has occurred.

The composition of the solution during the reactions and the degree of leaching (removing ions from environment) result in a particular clay mineral forming (Yong et al. 2012). Feldspar may weather to montmorillonite first and then to kaolinite, or directly to kaolinite depending on the conditions during weathering. Limited leaching environments that include non-draining profiles where cations are retained tend to form illite and montmorillonite, and where leaching favourable environments such as free-draining profiles tend to form kaolinite. However, with excess leaching of silica, iron, and aluminium oxides there tends to form minerals such as goethite and hematite, and gibbsite, respectively.

Throughout the weathering process the parent rock structure is largely retained, and for the relict rock structure to remain the original rock volume is also retained throughout most of the profile. Hencher (2012) stated residual soils above an igneous rock form when the original rock texture is lost and resulting material is typically a red, clay-rich, soil which will eventually collapse and densify through further weathering. The resultant macrostructure, porosity distribution and chemically constituents of the completely weathered bedrock is dependent on the parent rock characteristics, long term climate conditions and trends, prevailing moisture conditions in the profile, local vegetation and bioturbation, and regional topography. All the factors contribute to the type and intensity of weathering that occurs.

Formation of a weathered profile starts at the concept of a weathering front. A weathering front is assumed to be approximately parallel to the ground surface, however this is a simplification and is typically geometrically irregular (Phillips et al. 2019). Weathering is most intense at the ground surface and along rock fractures (i.e. joints and faults) and decreases with an increase in depth and reduction in jointing. As the weathering front moves down the ground profile, the degree of alteration increases towards the ground surface as indicate in Fig. 1.

This degree of weathering will usually result in a typical sequence of mineral occurrences with depth. The mineral which forms at a certain depth within a profile is dependent on the composition of the pore water, mineralogy of

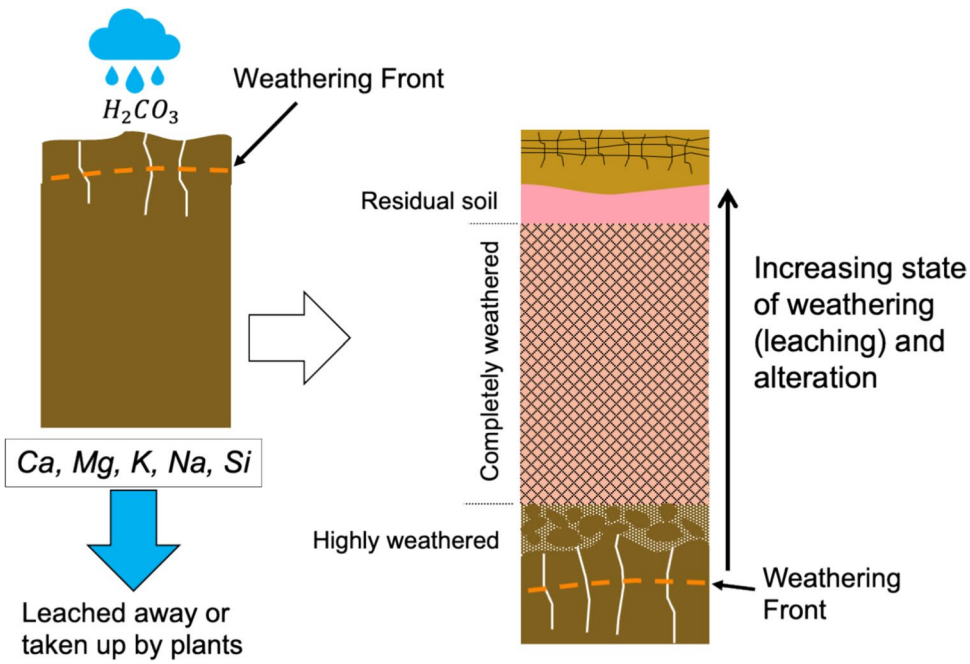

Fig. 1 Movement of weathering front forming typical soil profile

the parent rock, intensity of leaching and prevailing Eh–pH conditions at that depth (Summerfield 2014). Summerfield (2014) best represents the formation sequence of secondary minerals, based on leaching intensity (i.e., exposure time and depth in profile), from original primary minerals.

Generally, all feldspars and mafic minerals weather to kaolinite in free draining profiles in areas that class as Weinert N-value of less than 2 in Southern Africa (Weinert 1980). Usually following the path of primary mineral to montmorillonite to eventually kaolinite or directly decompose to kaolinite. Decomposition of primary mineral grains will vary in the profile, but generally increase from being a minimum in the parent rock and maximum in the upper residual soil. Additionally, Ca-rich feldspars and pyroxenes can completely dissolve resulting in an open pore while leaving no weathering products (Wilson 2004).

Chemical weathering indices are used to quantify the state of weathering by assessing the quantities of mobile ions such as Ca^{2+}, Na^{+}, and K^{+}, and the relative accumulation of immobile ions such as Fe^{3+} and Al^{3+}. Various methods have been put forward and successfully used in literature (Nesbitt and Young 1982; Fedo et al. 1995; Meunier et al. 2013; Liu et al. 2022; Cho and Ohta 2022; Sergeev 2023).

Many of these chemical weathering indices have their limitations and need to be adjusted based on the state of the weathered material and parent rock under investigation.

The most frequently used method to measure the degree of weathering is the chemical index of alteration (CIA). This method is based on the changes in chemical compositional associated with the decomposition of feldspar and formation of clay minerals. Since kaolinite is a common clay mineral into which most igneous rocks weather to, this method has been widely adopted (Cho and Ohta 2022). The CIA is calculated as presented in Eq. (1).

$$CIA = \frac{Al_2O_3}{Al_2O_3 + CaO^* + Na_2O + K_2O} \times 100 \quad (1)$$

CaO^* denotes the amount of CaO incorporated in the silicate fraction of the rock. The resulting value indicates the degree of weathering and typical values are between 30 and 45% for basalt, 45% and 55% for granites, and near 100% for kaolinite (Nesbitt and Young 1982). The range of the *CIA* for fresh rock is dependent on the chemical constitutions of the parent rock, and the calculated value has a possibility of reflecting a change in the source rock composition and not the degree of weathering (Meunier et al. 2013).

Meunier et al. (2013) proposed a method where the $M^{+}-4Si-R^{2+}$ system is used and takes the amount of silica into account, which the *CIA* does not. This method has been termed the weathering intensity scale (WIS) and estimates weathering by quantifying the loss in silica and the accumulation of less mobile elements during weathering (Bonnet et al. 2022). Each component of the $M^{+}-4Si-R^{2+}$ system is calculated, and the three values normalised to 100% and plotted onto a ternary diagram as stated in Meunier et al. (2013). Both the *CIA* and WIS methods can be successfully used for various igneous and sedimentary rock.

Cho and Ohta (2022) stated the *CIA* method has limitations due to chemical components used to calculate the degree of weathering. To fully utilise the method, the parent rock type and chemical data needs to be known which is often not the case. Therefore, a new weathering index method was derived and proposed, called the robust weathering (RW) method. The RW method can determine the degree of weathering of rock from a near fresh state to an intensely weathered, completely weathered rock and residual soil. The method does not make use of SiO_2, CaO, and P_2O_5 in the calculations but, of the six elements in the equation the largest influence to determine the weathering is the leaching out of Na_2O and accumulation of Al_2O_3.

The type of weathering to form deep weathering profiles is mainly the alteration of chemical components in the rock. The chemical and structural properties of the weathered material is closely linked and will evolve simultaneously as primary rock minerals change to secondary minerals, microcracks and openings will form, whereby increasing surface area and permeability to further the weathering process (Liu et al. 2022; Bonnet et al. 2022; Bonnet et al. 2023).

Throughout the decomposition of the parent rock, the structure is largely retained (Kellogg 1930; Schaetzl and Anderson 2005), however a weathered rock profile does undergo continuous volumetric strain as the degree of weathering increases (Banerjee et al. 2016; Hayes et al. 2019; Riebe et al. 2021; Liu et al. 2022; Dos Santos et al. 2022a, b; Bonnet et al. 2022; Bonnet et al. 2023). Chemical weathering of rock implies the alteration of primary rock minerals to secondary minerals, but also its physical properties such as total porosity, tortuosity of pore network, aperture of the pores and relative permeability, water flow, diffusivity, and mechanical strength will change. At the initial stages of weathering, micro pores will form as etching and defects along mineral cleavage breaks and imperfections (Wilson 2004). At macro scale, the knowledge of porosity evolution during weathering is one key parameter for predicting water storage capacity and water flow in the completely weathered and residual soil horizons (Bonnet et al. 2023).

Hencher (2024) stated residual soils above an igneous bedrock form when the original rock texture is destroyed through leaching out and transformation of parent rock minerals or volume change and densification due to collapse under self-weight. The resulting material is typically a red, clay-rich, soil with discontinuous, localised, zones having remnants of parent rock structure. This results in a reduction of the dry density as the weathering front pushes deeper into ground profile. As weathering depth increases the upper

portion of the completely weathered rock will collapse, whereby increasing dry density and reducing void ratio, destroying any existing relict parent structure, and forming residual soils (Hencher 2024).

Bonnet et al. (2022) study how the chemical weathering process impacts the Viamão granodiorite rock profile in South Brazil. The degree of chemical weathering, grain fragmentation, and development of connected porosity intensifies toward the upper layers of the completely weathered rock. Dissolution pits in feldspar grains form a network of intergranular micropores, while the expansion of biotite due to chemical weathering results in dense intergranular macrocracks. Both total porosity and macroporosity increase as you move upward in the completely weathered rock profile. Cracks formed during weathering and relict rock structure is often filled with clay and Fe-oxides. At the surface of the residual soil, grains become dislodged, causing the rock structure to break down and form a soil-like structure shaped by seasonal swelling and shrinkage cycles (Bonnet et al. 2022; Hencher 2024).

The relict rock structure and macro grain relations that survive the weathering process and persist in completely weathered rock provide strength and stiffness to the material (Wesley 1990; 2010; 2019; Bonnet et al. 2023; Wang et al. 2024). The relict rock structure can be lost through continued weathering in-situ, through rapid weathering once exposed to the Earth's surface and through anthropogenic influences (Obermeier and Langer 1986; Rabot et al. 2018; Dos Santos et al. 2022a, b; Liu et al. 2022). An oedometer test can be used to determine the influence the structure has on the compression behaviour of soil. When testing residual soils, the concept of the pre-consolidation pressure and over-consolidation ratio are not applicable as the material has formed through chemical weathering and not consolidation (Wesley 1990; 2010; 2019).

Wesley (2019) suggests the data should be plotted on a linear pressure scale and the soil compressibility should be determined. Examples of how oedometer data plots on a strain to linear pressure scale plot is presented in Fig. 2. Soil with structure is expected to yield if the yield pressure is reached underload and weaken. Non-structured soil is expected compress and strengthen as loading continues.

Rocchi et al. (2017) investigated the influence of weathering on the physical and mechanical properties of igneous rocks and found that the presence of the relict rock structure provided additional strength which decreased with an increase in weathering. The study also found that weathering generally causes a decrease in grain size as rock minerals decompose to clays and silts which reduces the shearing resistance of the material.

Hu et al. (2023) provided a comprehensive review of soil structural vulnerability, with a focus on how soil compaction and aggregate breakdown influence soil functions and

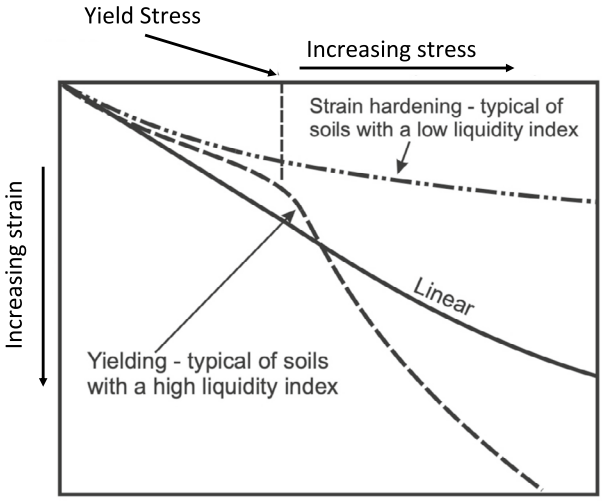

Fig. 2 Recommended analysis for soil compressibility behaviour when testing residual soils (adapted from Wesley 2019)

ecosystem services. A key factor affecting soil structural degradation is the pore network, which directly impacts soil functions like water and nutrient transport. The research proposes a model to clarify distinctions between susceptibility (inherent structural tendency to degrade), vulnerability (ability to resist stress under specific conditions), and risk (likelihood of degradation under real-world pressures). Soil structural condition is the measurement of the structure in-situ, and structural vulnerability is the possibility of the structure to alter due to external stresses. High resistance and resilience imply low vulnerability. The resistance reflects the ability of the soil to retain its structure when exposed to stress, namely continued weathering and the material being placed underload when the models are applied to completely weathered rock.

Obermeier and Langer (1986) found that highly decomposed completely weathered rock undergoes rapid weathering when exposed in an excavation, and the material can change from a medium hard rock to an extremely weak rock within 48-h. According to Hu et al. (2023) this material will be seen as having a high structure vulnerability. Townsend et al. (1969) and Saha et al. (2024) investigated the impact of destroying the soil structure and remoulding of soil samples have on the compressibility and strength of the material. Both studies found that breaking down the structure formed through pedogenic processes, results in a decrease in strength and an increase in compressibility.

Future research should concentrate on evaluating the connection between soil structural vulnerability and possible loss or changes in key soil functions indicators, such as the pore network and hydraulic conductivity.

Initially, the risk of soil structure degradation and the related changes in essential soil structure indicators, such

as hydraulic properties based on pore networks, should be assessed, taking into account soil structural vulnerability (Hu et al. 2023).

The characteristics of the completely weathered rock, especially the porosity, has been limited to breaking samples open to inspect 2D sections, simplified mass and volume calculations, and soil water retention curves among other techniques.

Letey (1991) wrote: *Science is based on quantitative measurements which can be reproduced. Soil structure does not lend itself to quantification*. He carried on stating the state of the art in the study of soil structure only provided index values for the soil functionality and these were dependent on how the functionality was measured (Letey 1991). At the time of writing up this study, the opportunities to measure soil architecture have significantly increased in the field of soil science (Golparvar et al. 2021; Daneshian et al. 2021; Vogel et al. 2022; Baveye et al. 2022; Wang and Zhang 2024).

Rabot et al. (2018) published a comprehensive review to evaluate the potential of observable soil structural attributes, for both the pore and aggerate approaches, to be used in the assessment of soil functions. As in geotechnics, the interest in soil structure is to infer the soil characteristics, which can form due to soil texture or chemistry (i.e. swelling / shrinking clays) or it may control the soil hydromechanical behaviour to a greater extent than the soil texture alone (Swart et al. 2019; Vogel et al. 2022; Baveye et al. 2022). Rabot et al. (2018) divided the methods into field and laboratory methods for the aggregate approach, and indirect and direct methods for the pore approach. Many of these methods were similar to techniques used in geotechnics to determine soil structure and porosity, such as test pit profiling in the field, and grading (texture) analyses and bulk density determination in the laboratory for the aggregate approach. In the pore approach, indirect methods discussed are gas adsorption and soil water retention curves and derived indicators, which is commonly used in unsaturated soil mechanics. Rabot et al. (2018) discusses the limitations and ambiguities in testing experienced when using the methods mentioned above, and some of these are similarly well-understood in geotechnics.

The direct methods for the pore approach include imaging techniques such as optical microscopy and scanning electron microscopy (SEM) (Rabot et al. 2018). These are commonly used in geotechnics, but these methods require sample preparation, such as cutting of thin sections, oven-drying and carbonization of sample surface that will disturb the soil structure before any evaluation takes place.

When analysing undisturbed soil samples to identify indicators of soil architecture, the most reliable and repeatable imaging technique is X-Ray Computed Tomography (XRCT) (Mees et al. 2003; Wildenschild and Sheppard 2013; Helliwell et al. 2013; Cnudde and Boone 2013; Banerjee et al. 2016; Rabot et al. 2018; Daneshian et al. 2021; Golparvar et al. 2021; Vogel et al. 2022; Baveye et al. 2022).

XRCT is a non-invasive, non-destructive, imaging technique developed for the visualisation and quantification of the interior structure of an object in the 3-dimensions. A sample is placed within the scanner and exposed to a beam of X-rays, generated from an X-ray tube, while the sample is rotated a full 360°. The X-rays are absorbed or scattered by, or passed through, the sample materials causing attenuation of the beam. The degree of attenuation is proportional to the atomic number of the material, the photon energy of the incident beam and the thickness of the material. The degree of X-ray attenuation is acquired by the detector from the numerous 2-dimensional (2D) radiographic images, often called projections.

The key principle of the XRCT imaging technique is based on the differential attenuation of X-rays as they interact with the minerals and pore spaces within the sample. The ability of differing materials to adsorb and scatter incident photons is referred to as the linear attenuation coefficient (Huda and Abrahams 2016). At a given photon energy and sample thickness, a higher density material (i.e. larger linear attenuation coefficient) will absorb or scatter more X-rays, increasing the attenuation, resulting in a darker appearance on the CT projection. Using relevant software depending on the application, the CT projection is converted into a slice where the denser materials appear lighter and air appears darker (Li and Tang 2019; Sturrock 2022). The process of X-ray attenuation in sample materials before photons reach the detector in a XRCT scanner is shown in Fig. 3.

Wang and Zhang (2024) provide a comprehensive review of soil pores and the importance on the soil structure, and how to measure them effectively. The paper provides methods to study pores and soil structure and categorizes them into traditional and advance techniques. The traditional methods are further divided into indirect and direct methods. Indirect methods include soil water retention curves, mercury intrusion, mathematical modelling and interpretation from permeability data. Direct methods include mainly observation of the soil at varying scales with the addition of tracer dyes and soil slicing. Although cost-effective, these methods can be limited by complexity and accuracy issues.

The most recent advances in imaging techniques includes XRCT scans that enable the quantification of porosity, pore distribution and pore connectivity. With the use of available image analysis software, such as VG Studio Max 2.2, the data retrieved during the CT scan can be used to determine number of pores, equivalent pore diameter, surface area and volume, as well as the 3D pore model reconstruction. The 3D model can be used to determine the pore tortuosity, connectivity, node density, and network density (Wang and Zhang 2024). Pore network modelling or pore scale modelling is used to create a relativity cost effective approach to

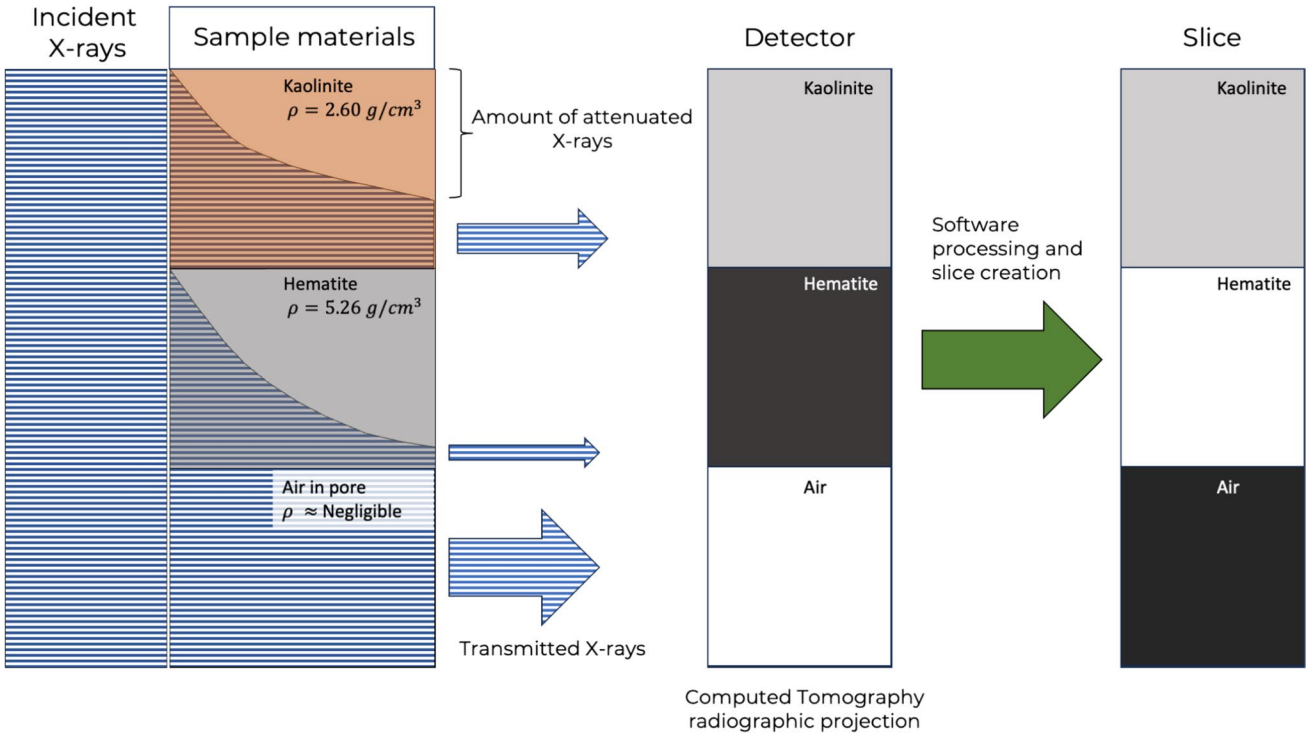

Fig. 3 X-ray attenuation contrast of solid mineral grains compared to open pore spaces in soil

characterise pore networks. XRCT scans have successfully been used to provide a basis for the microscale features to better characterize pore scale modelling (Blunt 2001; Golparvar et al. 2018; Wang and Rahman 2023).

Disadvantages do exist with this imaging technique notably the cost to hire and use the equipment and the availability of it as well. A limiting factor of the XRCT is the inability to differentiate between minerals with similar density near one another, as well as differentiating air and water in pores. To overcome this, sample preparation is required by means of an additive into the soil sample which stains certain soil features or pore water depending on the required application. The staining of specific features alters the density and enhances the contrast between certain minerals, liquids, or soil structures (Li and Tang 2019; Terribile et al. 2022).

The voxel resolution of the scan is dependent on the size of the sample and the size of the detector. Depending on the nature of the investigation, a suitable sample size and positioning of the sample relative to the detector and X-ray beam should be determined. By decreasing the distance between the sample and the X-ray source or increasing the distance between the X-ray source and the detector, the magnification increases. The shifting of these distances changes the magnification, which is inversely proportional to the field of view or allowable sample size. Therefore, the smaller the sample, the greater the magnification and higher the voxel resolution (Terribile et al. 2022; Wang and Zhang 2024).

No dedicated soil-based CT scanner or software exists and most XRCT research conduct on soil structure has been done using medical or industrial CT equipment as. For this reason, this method does not fully appreciate the irregularity and heterogeneity of the pore structure. Even with the disadvantages stated above, this imaging technique remains the most reliable and accurate of all widely used indirect and direct methods (Wang and Zhang 2024).

Methods and materials

Overview

The testing methods chosen for this research was aimed to investigate how the structure, which governs the porosity, changes through the weathering process and the implications it has on the material's mechanical strength. Undisturbed samples were taken at each sample depth and, sealed, wrapped, and stored in a manner to minimise loss of moisture and alteration of the structure as far as practically possible.

An oedometer was chosen to assess the influence of the presence and absence of relict rock structure in completely weathered rock and pedological features in residual soils due to its availability in industry, cost-effectiveness, and recommendation as stated in Wesley (1990; 2010). Placing

the undisturbed material underload will assess the vulnerability of the relict rock structure to resist alteration due to changes in the surrounding environment (Hue et al. 2023). Every undisturbed sample tested, was remoulded back to in-situ density, as similarly as possible and retested under the same conditions. A change in the behaviour and testing results were expected due to the influence of remoulding (Townsend et al. 1969; Hu et al. 2023; Saha et al. 2024). The remoulding of the material and testing under the same conditions will test the materials sensitivity. The state of weathering for each sample was determined using appropriate chemical weathering indices and therefore chemical components needed to be determined.

For limited samples as will be discussed, the porosity and structure of the samples was visually assessed in 2D and 3D by means of the X-ray Computed Tomography (XRCT) scan and associated software. The qualitative assessment was used to determine the state of chemical and physical conditions of the samples that was linked back to the degree of weathering.

The aim is to determine and compare the mechanical behaviour of samples taken from the same weathering profile, and how the state of weathering, presence of relict rock or pedological features, chemical constitutes, and pore geometry of the sample influence the expected behaviour.

An area along the eastern Great Escarpment of South Africa, located within the Mpumalanga Province, was chosen as the sample site due to the presence of completely weathered rock being exposed close to the natural ground surface. The top of the eastern escarpment represents an area where intensive chemical weathering and low erosion rates take place, and it is covered by a thin surficial transported horizon (Makhubela et al. 2021). This ground profile allows for accessibility to completely weathered rock material for sampling and logging in freshly dug trial pits.

The specific site on which the samples were successfully retrieved is underlain by the Dullstroom Formation of the Rooiberg Group. This geological unit comprises andesite to dacite, as well as rhyolites which are collectively referred to as the Dullstroom lavas. These volcanic units comprise fine-grained, groundmass with variable proportions of phenocrysts, porphyroblasts and amygdales. The Dullstroom Formation groundmass constitutes lath-shaped feldspar (mostly plagioclase), amphibole, anhedral quartz and opaque phases, including iron-oxide and ilmenite. The plagioclase can exist as phenocrysts characterised as euhedral to subhedral with composition of that of anorthite-rich (Ca-plagioclase) with minor albite (Na-plagioclase) (Schweitzer et al. 1995; Lenhardt and Eriksson 2012). The geological rock type will be classed in this research as an andesite for simplicity.

The trial pits at this site were dug at random until a weathering profile presenting completely weathered rock of the Dullstroom Formation was identified. The exposed ground profile at each location was logged according to the methodology as stated in Dippenaar et al. (2024) and Swart et al. (2023). The ground profile was either exposed in existing, recently dug, borrow pits, or exposed by means of machine excavation using an industry standard Tractor Loader Backhoe (TLB) (model: JCB 3DX or similar).

Laboratory tests

Particle size analysis and Atterberg limits

The samples underwent particle size analysis according to SANS 3001 GR1 (2013). The Atterberg limits testing was conducted using the one-point method as stated in SANS 3001 GR10 (2013). These two tests combined is commonly referred to in South Africa as a Foundation Indicator (FI) test. In this standard the liquid limit (LL) and plastic limit (PL) are determined using the Casagrande cup and the thread rolling method, respectively. The Atterberg limits testing was duplicated to ensure accurate readings were achieved. The laboratory Unified Soil Classification System (USCS) description was determined as stated in the ASTM D2487 – 17e1(2020).

Oedometers

One-dimensional consolidation testing is widely used and is seen as a fundamental soil behaviour test. The oedometer test applies a series of predetermined loads on to the sample and the deformation response is measured. The consolidation of a soil is dependent on its stress history, density, and porosity (Terzaghi 1943). Wesley (1990; 2010) recommends using the oedometer as a compression test to assess the fabric of residuum. The oedometer was chosen due to the availability in industry compared to the triaxial shear testing equipment at the time of writing this thesis. Lead times were more than 6 to 8 months and undisturbed samples were desiccated when removed from wrapping after standing for this period.

Humans frequently use the completely weathered rock in a profile as a founding medium and will apply loads that may or may not cause deformation to take place. Furthermore, the completely weathered rock is often ripped and recompacted at the founding level thereby changing the density and porosity. The change in volume will impact the porosity value and therefore flow characteristics of the soil and completely weathered rock profile.

Undisturbed samples were placed in an oedometer to undergo a one-dimensional consolidation test guided by the method stated in the BS 1377–5 (1990) code. These samples underwent a full compression test before the material was removed and remoulded to destroy any remaining soil

structure. The remoulded soil material was placed back into the oedometer cell and compacted to achieve the in-situ density. The remoulded porosity values and moisture content was brought as close as practicably possible to the in-situ values, however, due to the loss in structure, this was not always achievable. Therefore, the in-situ density value was governing parameter for the remoulded sample condition. The behaviour of the undisturbed and disturbed samples was assessed and compared in this study.

The interpretation of the oedometers was guided by the recommendations as stated in Wesley (2019). No attempt was made to determine the pre-consolidation pressure or over consolidation ratio. The data taken from the oedometer test results will be plotted on a linear stress strain curve to assess the compressibility of the soil (Wesley 1990; 2010; 2019).

The coefficient of volume compressibility (m_v) is defined as the volume change per unit volume per unit increase in effective stress. It defines the ratio of volumetric strain to applied stress of a soil and is the inverse of soil stiffness. Soil stiffness is also termed the constraint modulus (E'_{oed}) and is defined by Eq. (2) (Knappett et al. 2012).

$$E'_{oed} = \frac{1}{m_v} = \left(\frac{\mathrm{MN}}{\mathrm{m}^2}\right) = \mathrm{MPa} \tag{2}$$

The m_v value was used to quantify the stiffness the soil structure provided to the sample in the undisturbed state. It was also used to compare the difference in compressibility of the samples before and after remoulding.

XRF and XRD

The chemical compositions of each sample were determined by means of an x-ray fluorescence (XRF) spectroscopy which provides the elemental composition. X-ray diffraction (XRD) analyses were undertaken to provide information on the unit cell dimensions of the crystalline material in the soil.

The samples were tested at an accredited laboratory in Centurion, South Africa. The samples from each locality were milled and prepared in the laboratory.

The XRf samples were tested using the ARL ADVANT'X Series XRF instruments and Quantas software. The XRD samples were prepared according to the standardized Panalytical back loading system, which provides nearly random distribution of the particles. The samples were analysed using a PANalytical X'Pert Pro powder diffractometer in θ–θ configuration with an X'Celerator detector and variable divergence- and fixed receiving slits with Fe filtered Co-Kα radiation (λ = 1.789 Å). The phases were identified using X'Pert Highscore plus software. The relative phase amounts (weight%) were estimated using the Rietveld (1969) method.

X-ray computed tomography

The sampling methodology for X-Ray Computed Tomography (XRCT) samples comprised undisturbed block and tube samples. The tube samples were retrieved by pushing a PVC pipe (30.0 mm × 150.0 mm) into the sidewall of a freshly dug test pit. The tube sidewalls are approximately 3.00 mm thick, and no water loose is expected to occur through this. The tube ends were capped with 5.00 mm thick pipe stoppers. The sealed PVC tubes was then wrapped in plastic to ensure minimal moisture loss. Materials such as tin foil and other metals cannot be used as wrapping because these materials will distort the x-rays passing through the sample.

The tube samples were scanned at X-Sight X-Ray Services by means of their Nikon XT H225 ST system. The scans were conducted at 180 kV and 330 uA where approximately 2985 images were acquired of each sample while the samples rotated a full 360 degrees. Two-dimensional (2D) and three-dimensional (3D) slices were constructed using the Phoenix Datos acquisition and reconstruction software. The software processing focused on the sample material only and excluded a 2.00 mm space between the sample material and the tube's inner wall and 2.00 mm at the top and bottom portion of the sample. This was done to exclude areas where displacement and density alteration would have occurred at the sample and tube interface during sample retrieval. The density contrast and pore space analyses were performed with use of VOLUME GRAPHICS (VG) STUDIO MAX software.

As discussed in Sect. "Introduction", the behaviour of porous material is dependent on the 3D pore geometry and connectivity, which is directly linked to the parent rock and weathering intensity. The purpose of obtaining images using the XRCT scanner was to characterise the pore space orientation and size distribution, and the persistence of the relict rock structure and infill material of undisturbed samples. The scan could be done with no sample preparation, which ultimately sparse the structure and minerals from deforming or alternating during drying or saturation which is required in other imaging techniques.

After the tubes were scanned, the PVC pipes were cut open to assess the macro-relict-rock-structure. The same was done for the block samples. Finally, all samples were oven-dried to calculate the natural moisture content and dry density.

Results

Overview

The Dullstroom site is characterised by an open field with an existing 3.00 m to 4.00 m deep borrow pit present at

the site. A photograph of the borrow pit sidewall is presented in Fig. 4(a). The approximate depths of which the samples were taken is presented. It must be noted that these samples were taken in freshly dug pits as well as in the existing borrow pit sidewall. The test pits were dug at random until a well-developed weathering profile was observed. The 2D macro structure of the residual soil and completely weathered rock are shown in Fig. 4(b) and 4(c), respectively.

The residual andesite was logged as slightly moist, light orange, firm, open structured, fissured, silty clay. The completely weathered andesite was logged as moist, light orange blotched pink, stained black, extremely weak rock, jointed, relict rock structure, clayey silt.

Undisturbed block samples and disturbed bag samples were retrieved and sent to laboratory for appropriate testing. Four (4) tube samples were pushed into moist sidewalls, with one (1) in the residual and three (3) in the completely weathered rock with the general depth of each sample shown. The sample details were calculated using the tube sample data.

Sample 2835 represents the deepest and least altered of the completely weathered rock samples at the Dullstroom site. The tube samples were sent to the laboratory for XRCT scans.

Laboratory test results

Particle size analysis and Atterberg limits

The grading test results reveal that all samples, when completely broken down, grade as a sandy clayey silt with lesser and varying amounts of gravels. There is a general decrease in silt content with decreasing depth. The residual soil sample (2842) has the highest clay and sand content. The testing results for the particle size grading analyses and Atterberg limits is presented in Fig. 5.

Oedometers

The material was loaded at intervals of 6 kPa, 12 kPa, 25 kPa, 50 kPa, 100 kPa, 200 kPa, 400 kPa, 800 kPa, 1600 kPa as stated in the relevant standard. However, only the strain and void ratio between 6 and 800 kPa will be assessed. Analysing the behaviour of soil when under a loading of 1600 kPa is not a realistic scenario and testing results become unreliable at this stage of the test (Wesley 2010).

The strain curves for the undisturbed (Undis) and remoulded (Remo) samples retrieved at the Dullstroom site are presented in Fig. 6. The testing results summary for each sample is presented in Table 1. The value of mv is not constant for a soil but depends on the stress range for which it

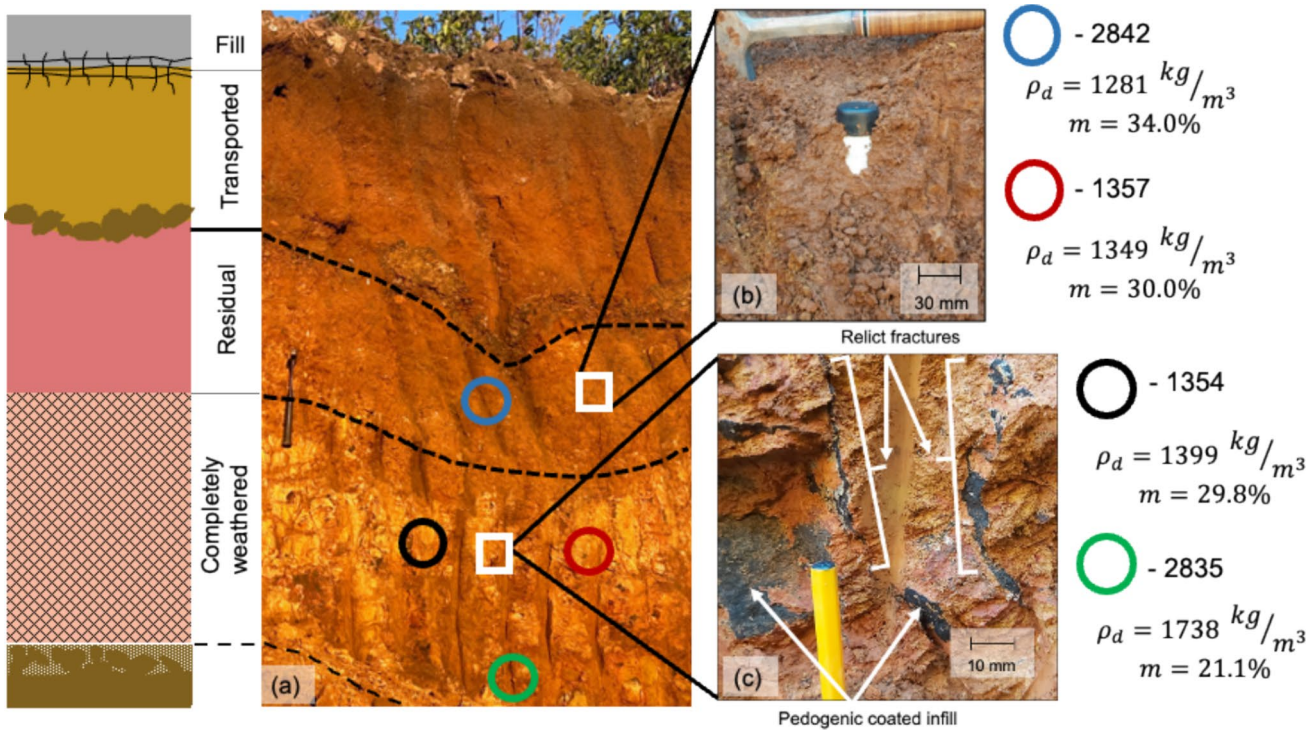

Fig. 4 **a** Existing excavation face at Dullstroom (photograph taken by MA Dippenaar); **b** Macro soil structure in residual soil with tube sample (**c**) Macro relict rock structure and pedogenic infill on relict fractures in completely weathered rock (photograph taken by D Swart)

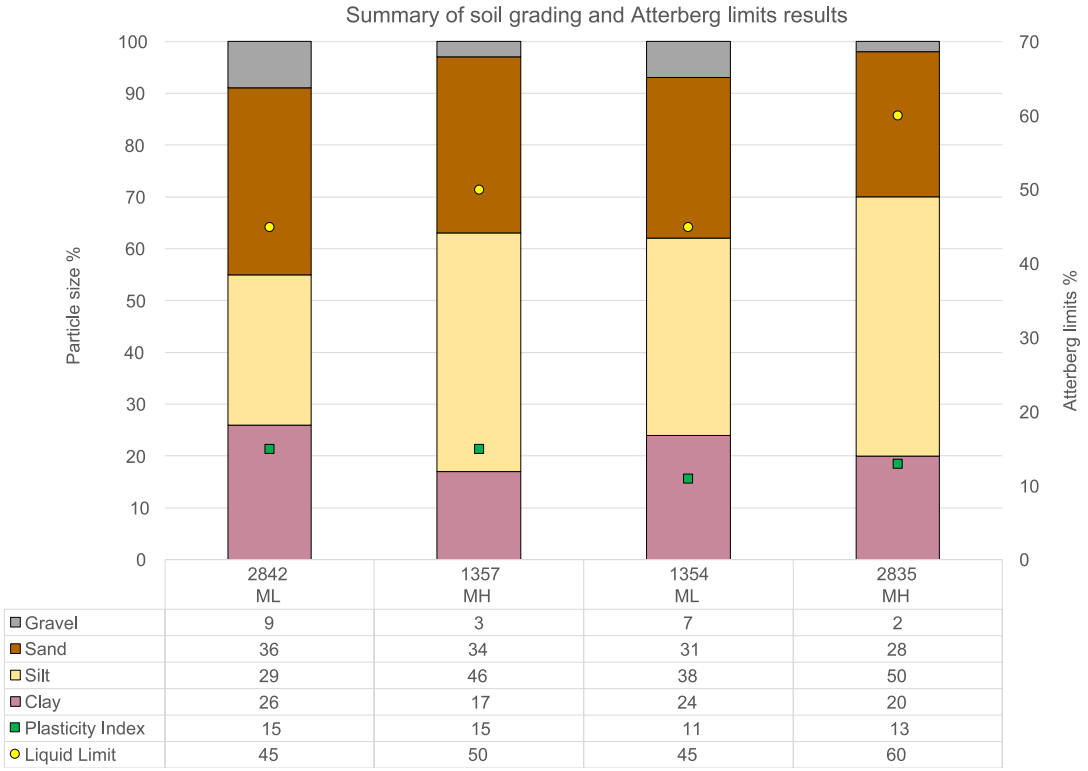

	2842 ML	1357 MH	1354 ML	2835 MH
Gravel	9	3	7	2
Sand	36	34	31	28
Silt	29	46	38	50
Clay	26	17	24	20
Plasticity Index	15	15	11	13
Liquid Limit	45	50	45	60

Fig. 5 Summary of particle size analyses and Atterberg limits

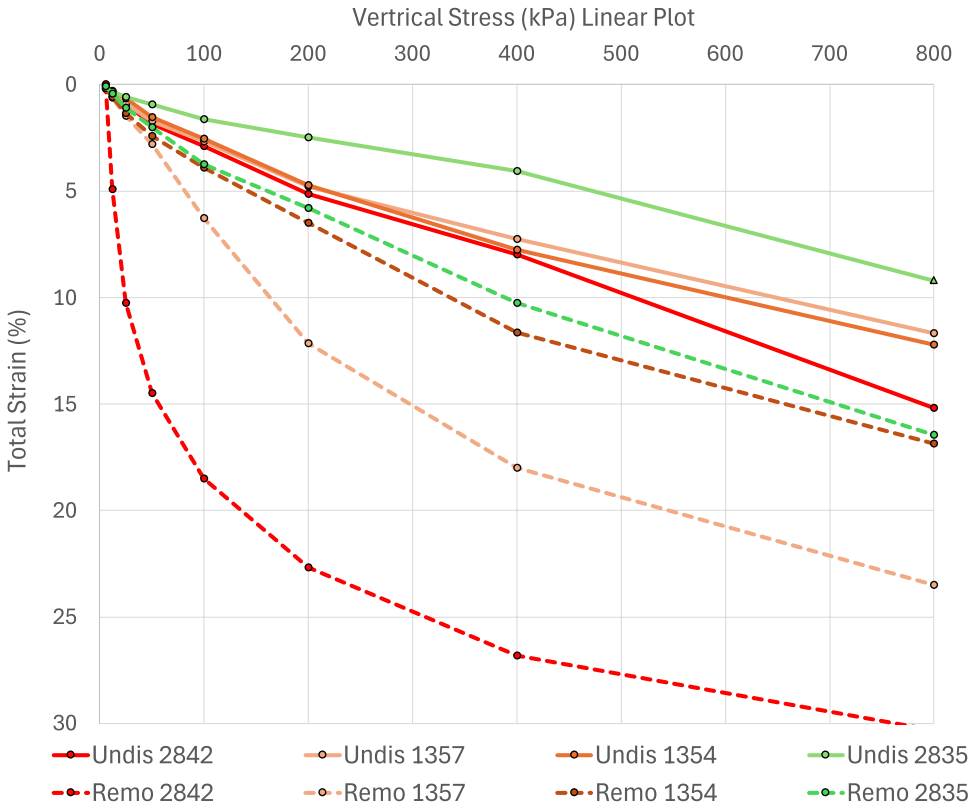

Fig. 6 Linear consolidation curves for undisturbed (Undis) and remoulded (Remo) samples

is calculated. It is calculated using data from the oedometer test results as the change in height can be measure with the change in stress known. Therefore, the mv value calculated for the stress increment between 50 to 100 kPa is given.

XRD and XRF results

The chemical testing, comprising the XRD and XRF analyses, was done to determine the weathering state of the samples. Only the required data to plot the chemical weathering indices are presented in Table 2. The XRD tests were conducted at numerous commercial laboratories and institutions. The interpretation of a mineral type is done by assessing *XRD* diffraction patterns and peaks, and these can shift and change due to amorphous crystal structures.

Less common soil minerals of similar structures or peaks are often grouped together with more common soil minerals, such as kaolinite and birnessite, and muscovite and lithiophorite, if no additionally testing is done to confirm the presence of either mineral (Swart et al. 2019). These limitations result in the XRD results to be influenced by operator bias. Notwithstanding, the Dullstroom XRD results were reviewed after the XRF results became available and the XRD results were updated based on the elemental composition. Only minerals, based on the XRF and XRD results, of significant importance to the study will be presented in Table 3.

X-ray computed tomography scan

The 2D slices and subsequent 3D porosity and density models were assessed, and figures produced using the VOLUME GRAPHICS (VG) STUDIO MAX software. The raw data is based on the density of the material scanned, and therefore a density colour contrast can be applied to identify the densest material in that sample. For continuity in analysing the samples, the upper 10% of the densest material was shaded in red when this method was applied. The orange shading was applied to the upper 20% of the densest material. The results for the least weathered sample 2835 will be presented first and progressively working towards the most weathered sample 2842. It must be noted the smallest pore that could be modelled for the Dullstroom samples was 0.16 mm equivalent diameter.

Figure 7(a) shows the 2D slice of sample 2835 from the top view and right view with the cross-sectional plane of the top view indicated. The yellow markers indicate a well-defined, tight, fracture of the relict rock structure present in the sample that persists both laterally and horizontally through the sample. The yellow brackets show the orientation of the same specific structure in the two adjacent

Table 1 Oedometer testing results summary

Sample ID	Dry density (kg/m^3)		Void ratio		m_v (1/MPa) at 100 kPa	
	Undisturbed	Remoulded	Undisturbed	Remoulded	Undisturbed	Remoulded
2842	1114	1065	1.542	1.579	0.216	0.985
1357	1160	1083	1.273	1.615	0.193	0.716
1354	1285	1252	1.078	1.134	0.209	0.299
2835	1012	1170	1.729	1.253	0.140	0.354

Table 2 Summary of XRF test results

Sample ID	Weight percentages (wt.%)								
	SiO_2	Al_2O_3	Fe_2O_3	MgO	MnO	CaO	K_2O	P_2O_5	Na_2O
2842	57.0	16.3	14.9	0.46	0.25	0.03	0.53	0.31	0.01
1357	47.9	28.1	11.9	1.22	0.11	0.07	1.81	0.25	0.01
1354	46.5	29.6	11.6	1.29	0.08	0.07	2.38	0.24	0.01
2835	56.5	25.9	9.43	1.70	0.06	0.12	4.46	0.31	0.12

Table 3 Summary of XRD test results

Sample ID	Weight percentages (*wt.%*)					
	Quartz	Kaolinite	Microcline	Gibbsite	Muscovite	Goethite
2842	55.5	37.8	-	-	4.90	1.80
1357	24.4	32.3	1.10	0.7	19.3	0.10
1354	25.6	34.5	2.10	-	10.9	0.02
2835	20.5	24.1	12.7	-	15.6	0.04

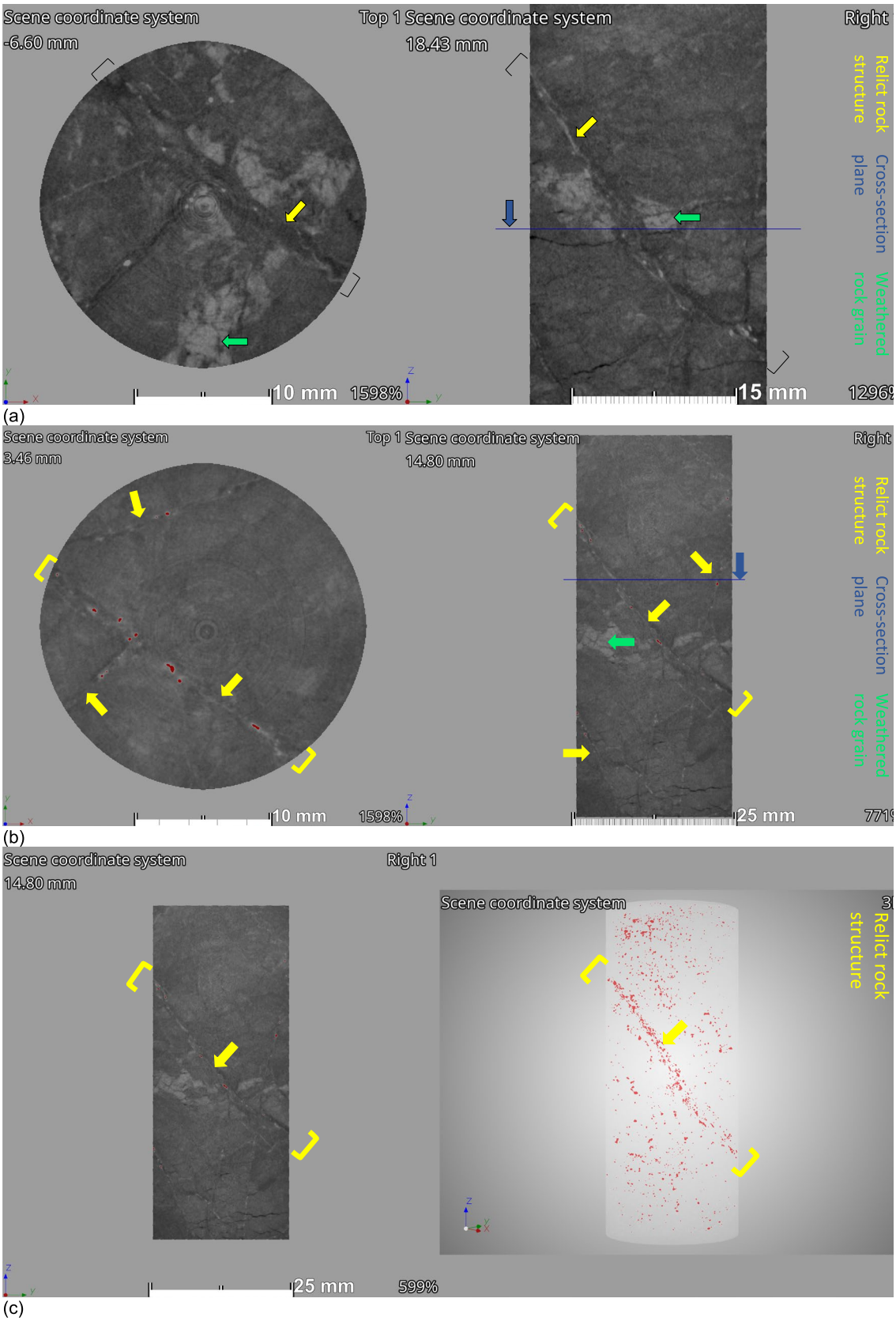

Fig. 7 **a** Sample 2835 2D slices from top view (left) and right view (right); **b** with density colour contrast; **c** 3D distribution of denser minerals

images. Weathered rock grains, most likely microcline according to the chemical testing results, which are slightly denser (lighter) than the surrounding material less dense (darker) clay present. The difference in densities of the individual minerals allows for colour contrasts to be created based on relative density to the lowest density material in the sample. In Fig. 7(b) the denser minerals are highlighted in red and occur as discontinuous pockets within the relict rock structures and are denser than the weathered rock grains. To further evaluate the occurrence of the denser material, a 3D density contrast is presented in Fig. 7(c).

Figure 8(a) and (b) presents the 2D slices and 3D models for sample 1357 with the density contrast applied and indicates a horizontal and vertical structure, respectively. The 3D porosity model is presented in Fig. 9(a) and shows the pore geometry is governed by structural orientation of the completely weathered rock. The top view in Fig. 9(b) shows the pore orientation to be parallel to the vertical

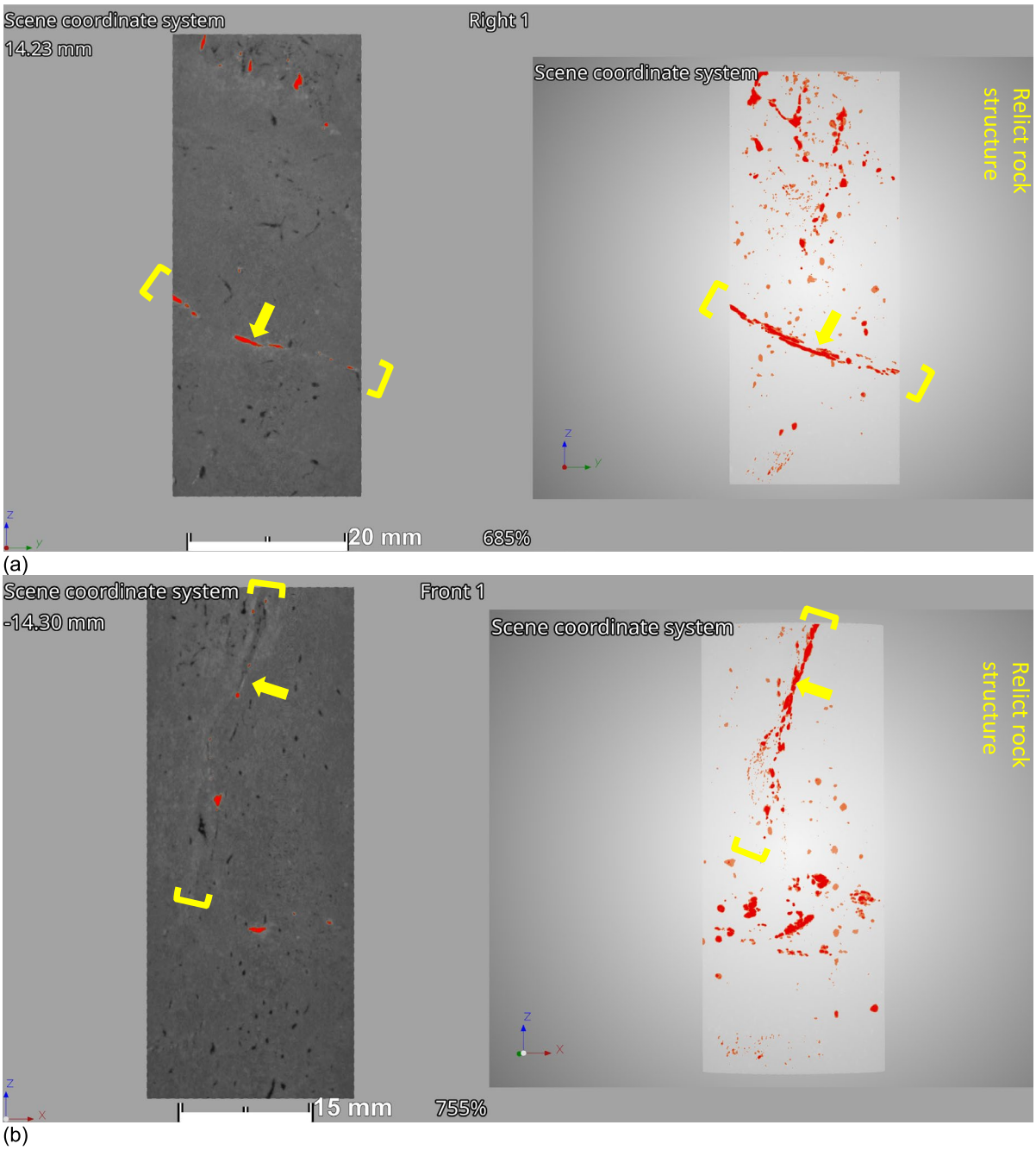

Fig. 8 **a** Sample 1357 2D slice right view (left) and 3D density contrast (right); **b** front view (left) and 3D porosity distribution (right)

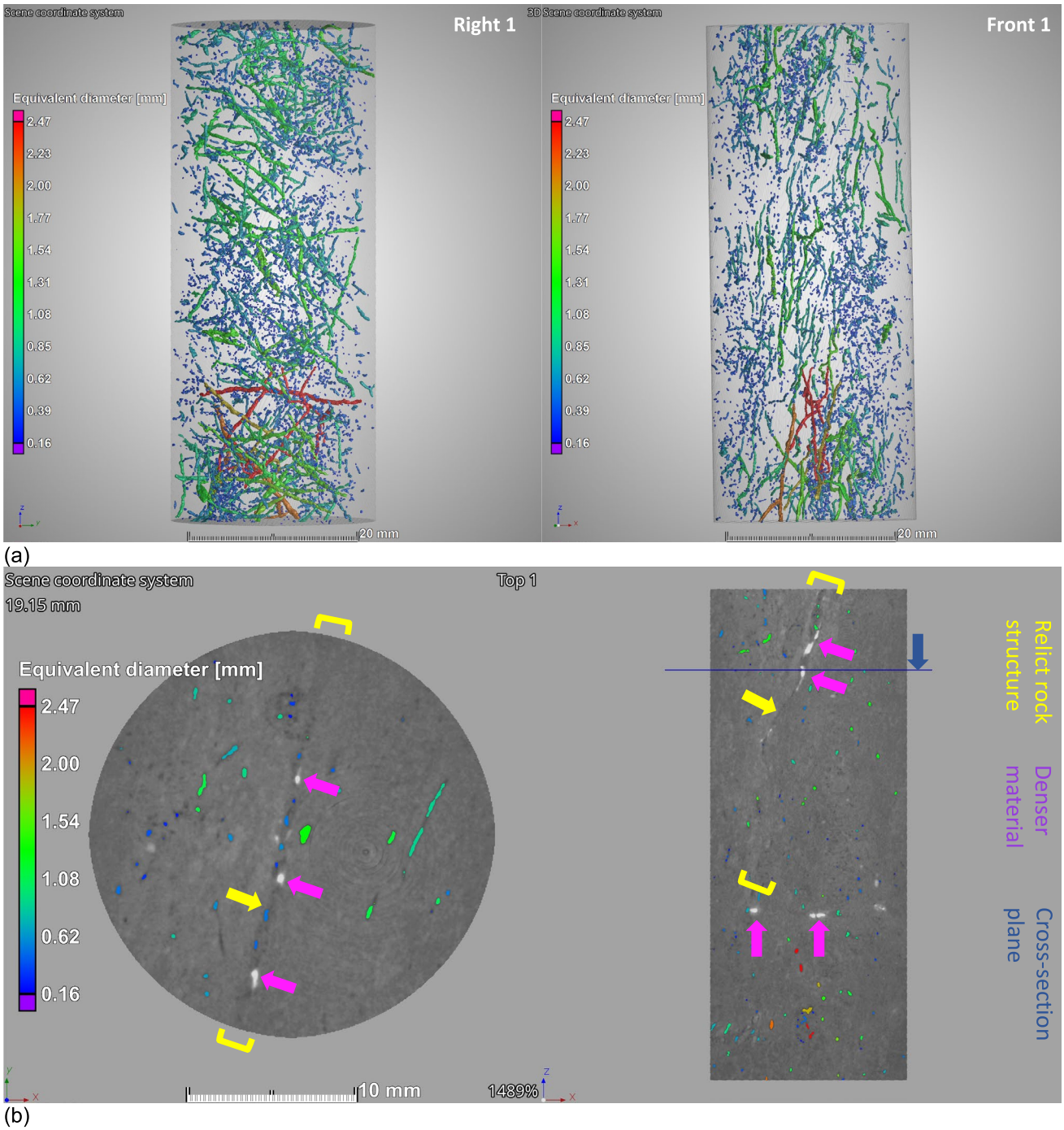

Fig. 9 **a** Sample 1357 3D porosity model with right view (left) and front view (right); **b** with 2D slice overlay top view (left) and front view (right)

structure identified in this sample, as well as showing the structures comprising open pores and pedogenic material. The matrix has a more uniform greyscale, compared to sample 2835, with no indication of weathered rock minerals, suggesting all minerals in this sample have weathered to secondary clays and weathered quartz.

Figure 10(a) and (b) show denser pedogenic formations in possibly a relict rock fracture that has eroded and changed shape over the weathering process. The density contrast has been stacked in Fig. 10(b) where the red is the densest and orange is slightly less dense. This was done to see if the denser material exists in the completely weathered rock

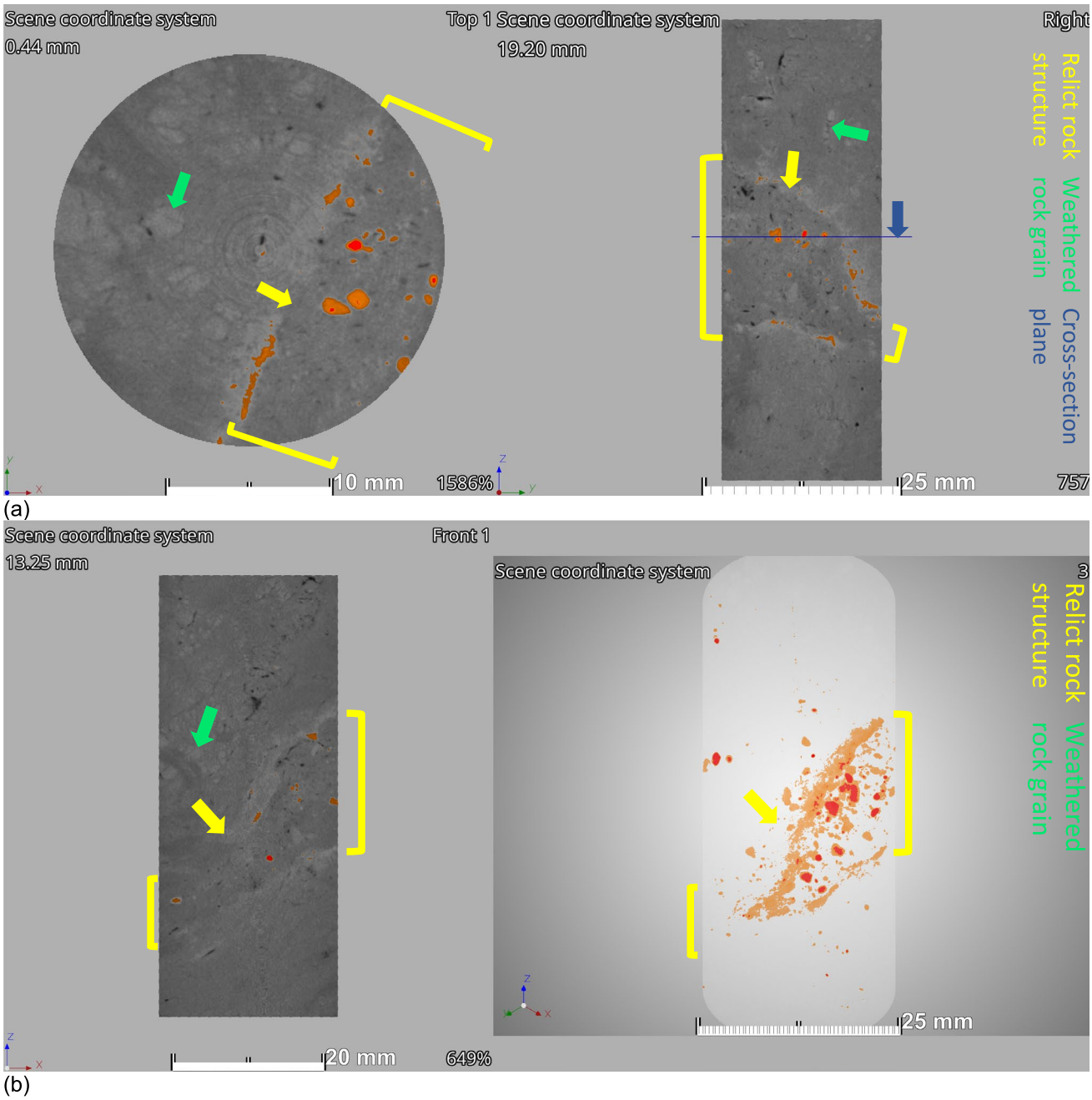

Fig. 10 **a** Sample 1354 2D density contrast with top view (left) and right view (right); (**b**) with 2D slice front view (left) and 3D density contrast (right)

matrix. The weathering has resulted in relatively thick infill material. This fracture could have formed through volumetric strain during the weathering of an existing major joint that was a preferred flow path in the original parent rock mass. The staining of metal oxides on the joint faces indicates this formation is naturally occurring and has not formed as a result of sampling disturbance. The denser material occurs as 1.00 to 2.00 mm, rounded, nodules in the infill material with portions of the facture sidewall having pedogenic coatings. Other, subrounded to sub-angular grains can be seen in the infill material. Within the completely weathered rock matrix, weathered rock grains can be seen with very little to no material being highlighted in the density contrast. This sample provides a distinction of fabric characteristics of completely weathered rock and infill material within a possible preferred flow.

The 3D porosity model is shown in Fig. 11(a) and reveals there is a preferred pore orientation within the

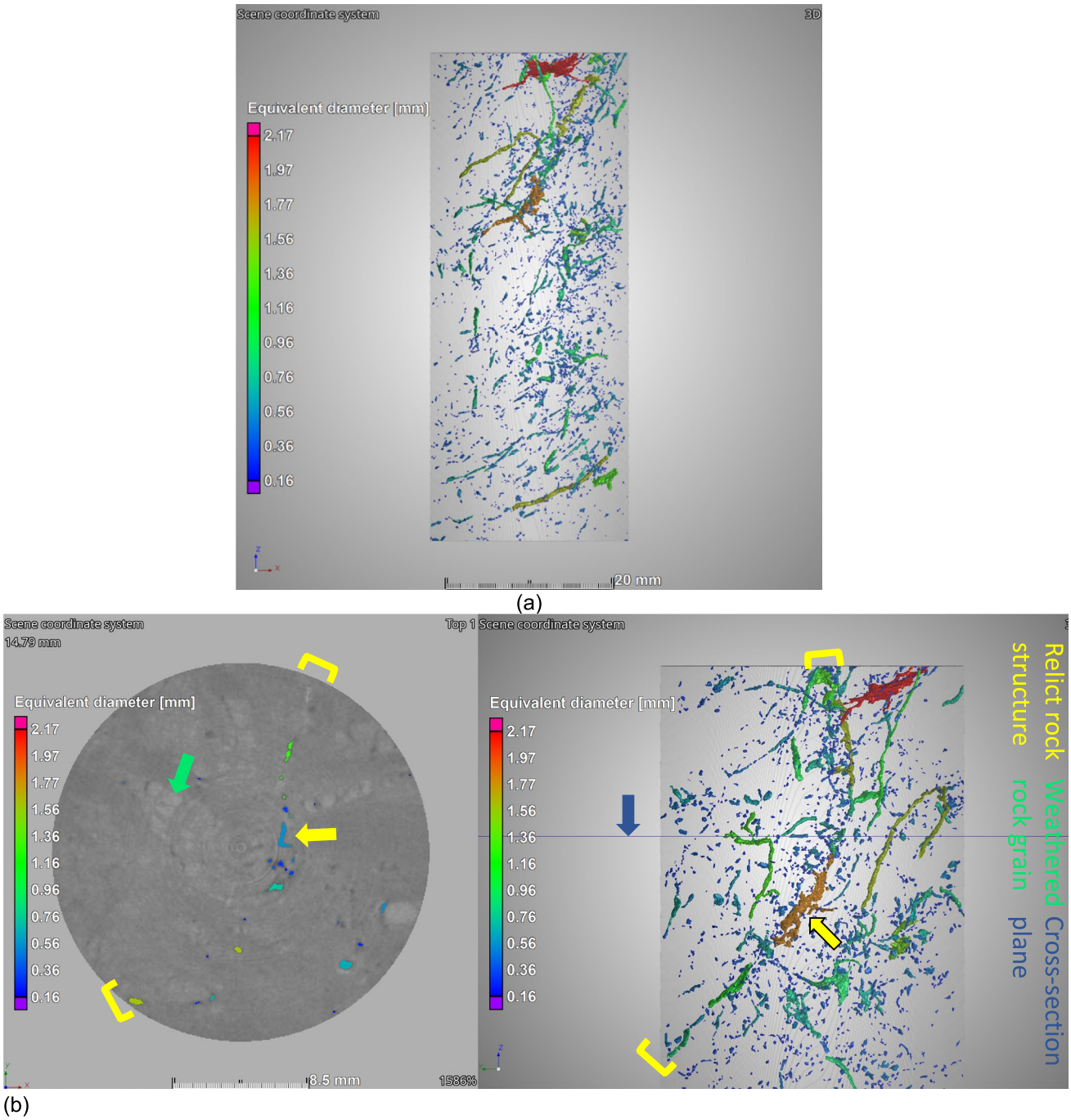

Fig. 11 **a** Sample 1354 3D porosity model; **b** from top view (left) and 3D porosity model (right)

sample that follows the same direction as the infilled fracture. Focusing on the top portion of the sample, a distinction can be made on a possible open fissure as shown in Fig. 11(b). Here the fissure forms a series of connected and disconnected pores with no indication of dense material within the structure itself. It is expected the fissure has recently opened due to volumetric strain during weathering and therefore there has not been enough time for pedogenic deposits to occur within this fracture. The fissure is curvilinear in shape in both the vertical and horizontal directions.

The 2D slice with the density colour contrast and 3D density model for sample 2842 is shown in Fig. 12(a). The sample has lost the majority of the relict rock structure and the pedogenic deposits are mostly rounded and do not follow or exist within a defined relict rock structure. A partial

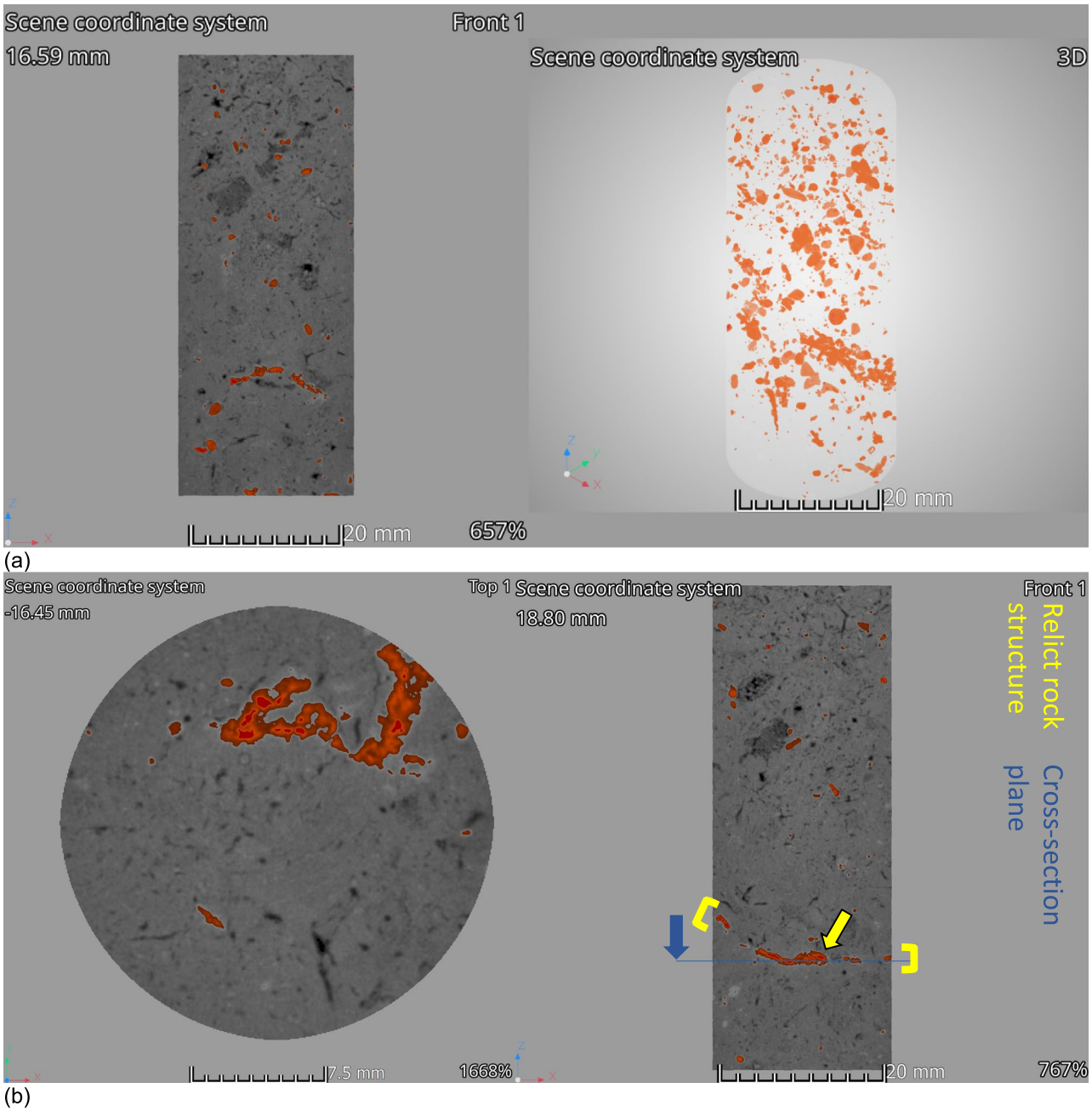

Fig. 12 **a** Sample 2842 2D slice from front view (left) and 3D view with density contrast (right); **b** from front view (left) and 2D density contrast (right)

relict structure in the lower portion of the sample persists and is shown in Fig. 12(b).

Figure 13 reveals how highly voided the most weathered sample 2842 is compared to the less weathered samples retrieved from the same profile. The largest void, shaded in red, is seemingly a root that has propagated through the matrix and created an open root channel. The 2D slices and 3D models indicate the residual soil has lost the original rock structure that is maintained in the completely weathered rock.

The smallest effective diameter recorded in all samples was 0.16 mm. According to Brewer (1965) and updated by Bouma (1981) these pores will class as macro-pores, where micro pores are 0.03 to 0.005 mm in diameter. This resulted in many of the pores smaller than 0.16 mm to be excluded from the 3D porosity model. The sample size caused the

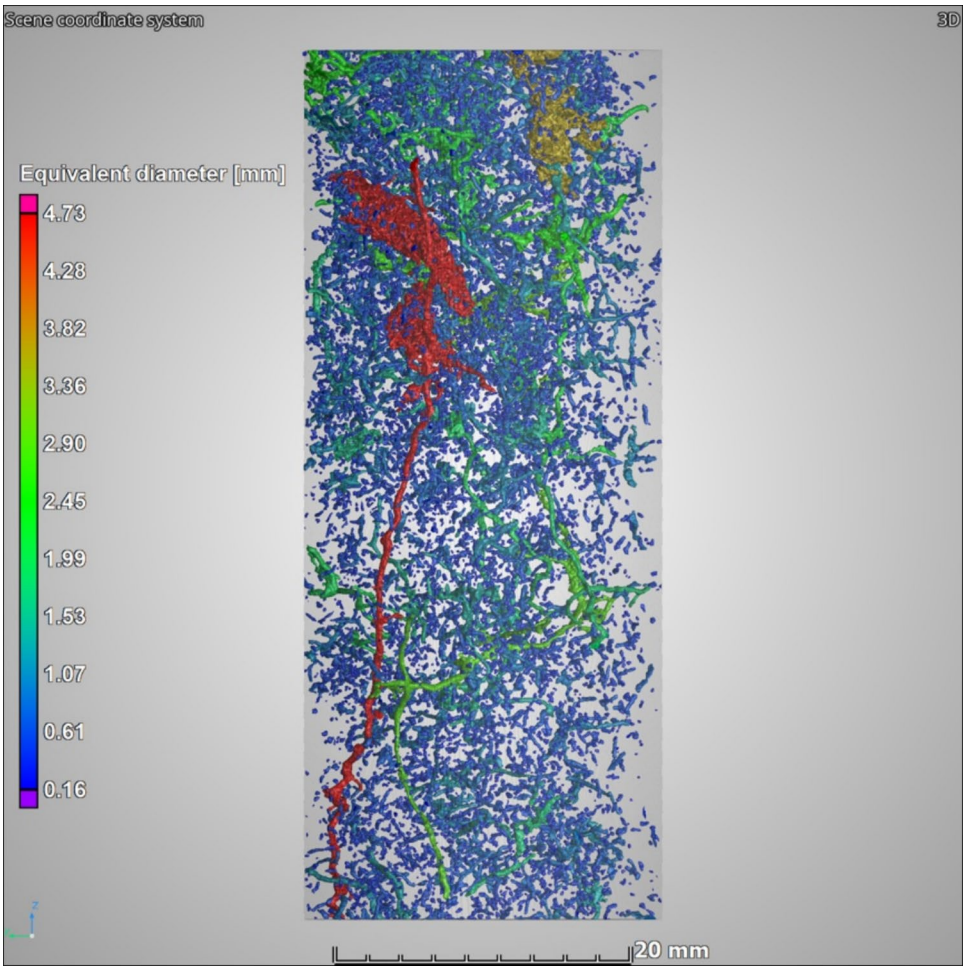

Fig. 13 Sample 2842 3D porosity model

field of view to be large which is inversely proportional to the resolution and therefore results in large pixel sizes. The voxel resolution of the scan is dependent on the size of the sample and the size of the detector. By decreasing the distance between the sample and the X-ray source or increasing the distance between the X-ray source and the detector, the magnification increases. The shifting of these distances changes the magnification, which is inversely proportional to the field of view or allowable sample size. Therefore, the smaller the sample, the greater the magnification and higher the voxel resolution (Sturrock 2022). This study then investigated the macro pores only. However, for engineering purposes, this will be sufficient as most geotechnical problems and concerns stem from the macro pores which is seemingly controlled by the relict rock structure. The mesopores and micropores distribution and geometry becomes essential for hydrological studies.

A limiting factor of the XRCT in this study was the inability to differentiate between minerals with similar density near to one another, as well as differentiating air and water in pores. To allow for better differentiation, sample preparation is required by means of an additive into the soil material which *stains* certain soil features or pore water depending on the required application. The *staining* of specific features alters the density and enhances the contrast between certain minerals, liquids, or soil structures (Li & Tang 2019; Terribile et al. 2022). The main aim of this study was to characterise the in-situ soil structure and mineral relation at different weathering stages and sample preparations may have had an impact on these.

XRCT scans can be successfully used to assess the presence of structure in a soil material without the need to dry out the material or any other destructive sample preparation steps. It can provide information such as pores geometry in 2D and 3D, persistence of structure, and typical moisture flow paths. Depending on the sample size, the pores' structure can be confidential modelled based on the voxel data. It must be stated that final 3D porosity model is a theoretical model of the pore structure based on many factors. The method is considered an indirect measurement of soil structure as it is dependent on the voxel size, which is influenced by strength of XRCT, sample size, operator effectiveness.

Discussion

The state of weathering of each horizon encountered in the igneous weathering profile during this study will be assessed based on the chemical weathering indices recommended in literature, namely the chemical index of alteration (*CIA*) and weather intensity scale (*WIS*).

The Dullstroom site comprised three (3) samples taken from the completely weathered rock. Samples 1354 and 1357 were taken near the completely weathered rock and residual soil interface, and sample 2835 was taken approximately 4.00 m below ground surface and is considered the least weathered of all the samples. This was done to visually assess the influence of weathering within the same horizon, based on geotechnical parameters, on the structure. The structure was easily broken down by moderate pressure from fingers into a silt, as shown in * MERGEFORMAT Fig. 14. Note the black staining on the joint surfaces.

The chemical and visual assessments revealed the rock comprised primary rock minerals such as microcline. The light grey shaded areas in the XRTC scan are most likely decomposed microcline mineral. The black and dense material in the joints of sample 2835 is most likely goethite as this has a higher density at 3.8 g/cm3 compared to the microcline at 2.6 g/cm3. Goethite can form through pedogenic

Fig. 14 **a** Sample 2835 with structure intact (**b**) Sample 2835 after smeared with light finger pressure (photographs taken by D Swart)

processes in preferred moisture flow channels such as joints (Van der Merwe 1964; Banerjee et al. 2016). The pedogenic deposits almost always occurred in the relict rock joints in the completely weathered rock. Assessing the tube sample material and the XRCT imagery, it is evident that the structure becomes less prominent with increased weathering when moving up the profile. The pore distribution generally stayed in orientation to the major rock fractures in all the completely weathered samples.

Figure 15(a) indicates that all the completely weathered rock samples excavate as a silt mixture and the residual soil has slightly higher clay content and plasticity. This agrees with the XRD results that showed a higher quantity of kaolinite and no primary rock forming minerals. This is expected for a more weathered soil, as shown Fig. 15(b) (Van der Merwe 1964; Bonnet et al. 2022; Wang et al. 2024).

The XRCT imagery showed the material lost all relict rock structure and the pore structure was governed by pedogenic and biotic processes. According to the tube samples the dry density decreased as weathering increased moving up the profile, as shown Fig. 4. However, according to the oedometer samples, the completely weathered rock had lower than expected dry density which was lower than the residual soil. This may have occurred for a few reasons, namely a less dense pocket was sampled in the completely weathered rock.

It is expected that the completely weathered rock would have undergone a greater amount of strain since the initial parameters had a lower dry density and a higher initial void ratio compared to the residual soil. However, as can be seen in the oedometer results in Fig. 6 and Fig. 15, the completely weathered rock experienced less strain than the residual soil both for the undisturbed and remoulded samples. The structure in the undisturbed 2835 sample provided the stiffness to limit the total strain experience. Once the structure was lost through remoulding, the 2835 sample underwent a greater amount of strain compared to the residual soil undisturbed sample.

Figure 16 presents plots for the coefficient of volume compressibility (m_v) against the sample's dry density (ρ), void ratio (e) and degree of weathering determined by the *CIA* and *WIS* methods. Typically, for soils that formed through consolidation and Terzaghi's (1943) theory of one-dimensional consolidation can be applied, many of the equations to predict compression of soil is based on the void ratio (Fukue and Okusa 1987; Al-Khafaji and Andersland 1992; Wu et al. 2024). Figure 16(a) and (b) plot the m_v against the dry density and void ratio, respectively. As can be seen the data is fairly scattered with no relationship being shown between the compressibility of the soil and the density and volume parameters.

Referring to Fig. 16(c) and (d), which plots the degree of weathering to the compressibility of the soil, a relationship does seem to appear. It must be noted that no correlation will be attempted to be made as the data set is limited. It seems the degree of weathering is a better predictor for compressibility of residuum than using initial void ratio or dry density due to the presence of the structure. The stiffness provided by the relict rock structure has been shown in this research and by many other authors. This positive influence has been shown to decrease with an increase in weathering (Rocchi et al. 2017; Jacques et al. 2021; Liu et al. 2022; Bonnet et al. 2023; Wang et al. 2024).

The XRCT scans conducted in this study showed the most *prominent* relict rock structure is present in the least weathered igneous rock and this *prominence* decreases with an increase in weathering until the structure is eventually destroyed to form the residual soil higher up the profile. This trend was confirmed by the chemical analyses, which was used to determine the degree of weathering. The compressibility of residuum, being residual soil and completely weathered rock, forming on igneous weathering profiles is expected to increase with an increase in weathering and subsequently a decrease in relict rock structure *prominence*.

Figure 17 presents a photograph taken of completely weathered andesite with high structural *prominence*. The structural *prominence* should be treated a single parameter that can be used across different geologies and weathering profiles. The photographs presented are of completely weathered rock originating from different parent rocks at different rates of decomposition due to the differences in climate history. All these specimens have varying void ratios and dry densities, but all have high structural *prominence*. High structural *prominence* is characterised by the presence of inter-grain relations and fractures or joints that are inherited from the parent rock. The structural *prominence* decreases when all primary rock-forming minerals have fully decomposed, microcracks form through the fabric, and pedological processes start to form and influences the pore spaced of the material. These features should be assessed on a range of scales from micrometres to centimetres. The structural *prominence* can be assessed visual by hand samples, XRCT scans, and it can be quantified using chemical weathering indices as discussed in this research.

Figure 18 shows the decrease of structural *prominence* with an increase in chemical weathering. The photographs are of tube samples that have been cut in half along the longitudinal axis and the two halves separated with the sampled material being allowed to break apart along pre-exists cracks or fractures, or through the soil fabric. Referring to sample 2835, the material has a structural *prominence,* and primary rock-forming minerals and texture can be seen with staining on relict fractures along which the sample broke part. Sample 1354 exhibits relict rock structure with a significantly more quantity of pedogenic nodules and microcracks that have formed in the soil due to weathering. These features

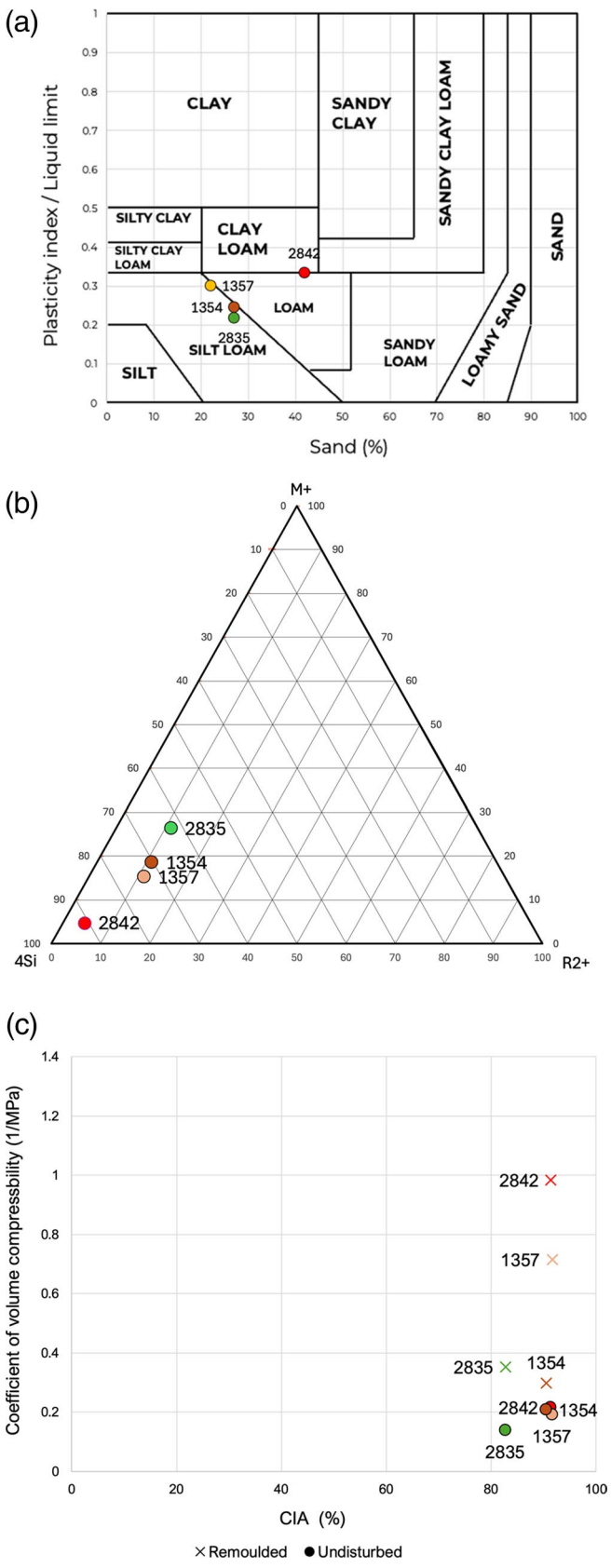

Fig. 15 **a** Texture classification (Moreno-Maroto and Alonso-Azcárate 2018; 2022) (**b**) Weathering intensity scale (*WIS*) (Meunier et al. 2013) (**c**) m_v value calculated for stress increment from 50 to 100 kPa vs chemical index of alteration (*CIA*) (Nesbitt and Young 1982) for the Dullstroom samples

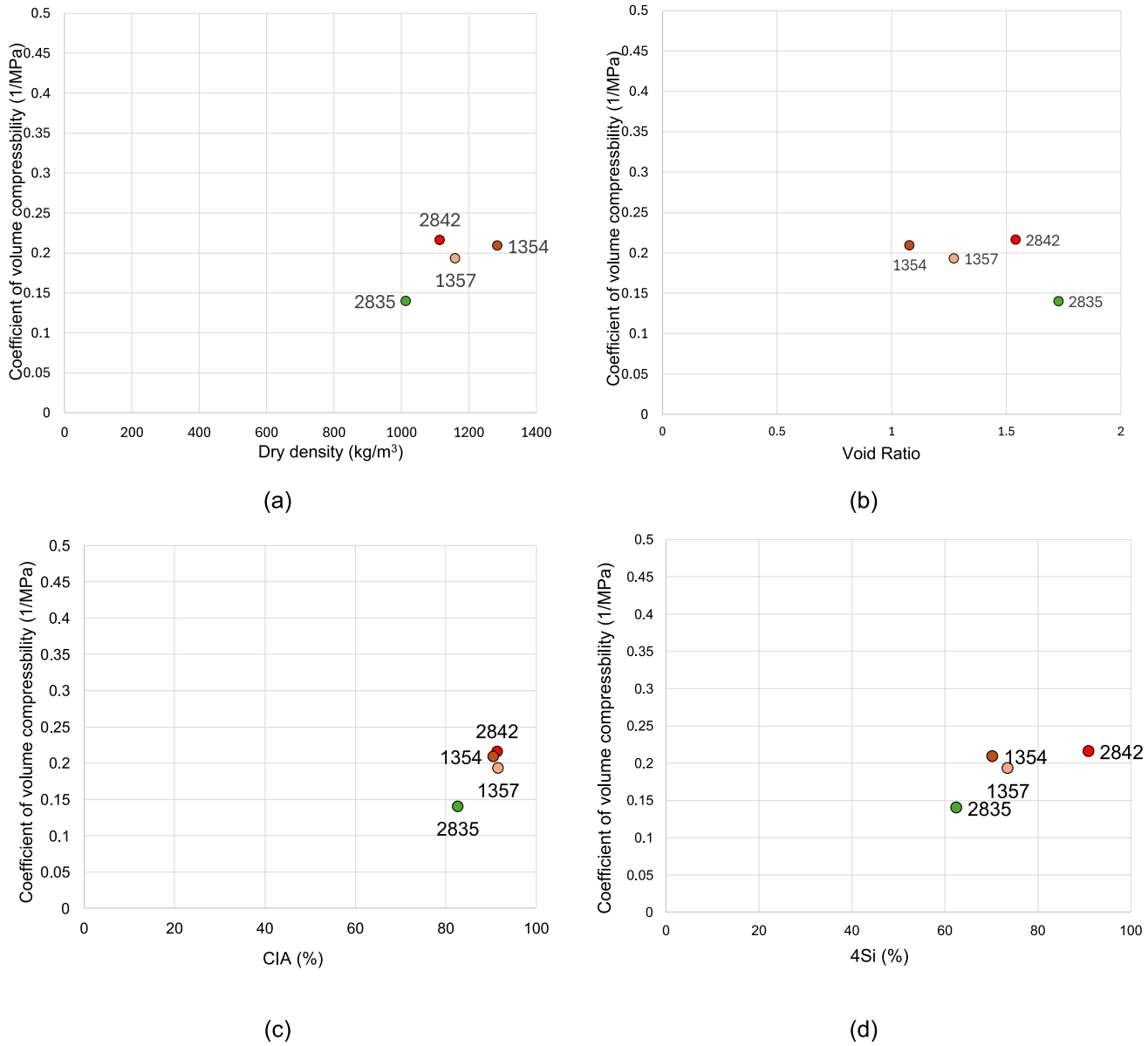

Fig. 16 The m_v value calculated for stress increment from 50 to 100 kPa plotted against (**a**) dry density, (**b**) void ratio, (**c**) chemical index of alteration value (*CIA*), and (**d**) 4Si value from the weathering intensity scale (*WIS*) for Dullstroom samples

were confirmed in the XRCT scans. Sample 1357 has broken along a relict rock fracture and exhibits a weak relict rock structure. Open root channels and flow channels can be identified from the XRCT scan and on the photograph. Sample 1354 and 1357 are considered to have moderate structural *prominence*. Sample 2842 is a sample of the residual soil and mostly comprise reddish clay with discontinuous relict rock structure zones in the lower half of the photograph. The soil structure will be controlled by pedological processes and biotic activity, and therefore this sample has lost the structural *prominence.*

It is proposed to use the concept of structural *prominence* when assessing the influence of relict rock structure on the material's mechanical performance. This study focused on compression behaviour for one (1) weathering profile only with very limited data points and information from literature. This concept is only an introduction to the idea to create a single parameter to include the influence of geological processes occurred during weathering. Further studies would need to be conducted using more elaborate triaxial shear testing equipment across multiple weathering profiles on various rock types. This concept is put forward to create

Fig. 17 Photograph taken of completely weathered andesite sample 2835 (photographs taken by D Swart)

opportunity to assess the mechanical behaviour of influences by the relict rock structure and the state of weathering. Figure 19 visually illustrates changes to the structural *prominence* in a weathering profile and how it influences the compression of the material. For this simplified weathering profile, the structural *prominence* is higher deeper in a profile where less weathering has occurred. Structural *prominence* can exist in a discontinued state in the residual soil in some cases, however, more work focusing on this would need to be done to confirm how far up into the residual soil it is present and under what conditions would this occur. Pedological features are structures formed through typical soil forming processes. This research has shown that these features, namely pedogenic nodules, biotic activity and fissures and cracks, do exist within the completely weathered rock. Pedological features is included in this schematic to show how it increases into the residual soil and mostly governs the residual soil's structure as weathering continues. The compressibility decreases with an increase in weathering and decrease in structural *prominence*. The dashed lines indicate the path the parameter will most likely follow in a weathering profile; however, the actual path will depend on numerous factors that are variable to the point where it would change from profile to profile.

Conclusion

XRCT scans offer a reliable, non-destructive method to evaluate soil structure without requiring drying or other invasive sample preparation steps. They provide valuable insights into pore geometry in both 2D and 3D, the persistence of structural features, and potential moisture flow paths. The pore structure can be effectively modeled in 3D based on voxel data, depending on sample size and resolution. However, it is important to note that the resulting 3D porosity model is a theoretical representation influenced by factors such as voxel size, the strength and settings of the XRCT scanner, and operator proficiency. Despite being considered an indirect measurement, XRCT remains a robust tool for characterizing soil structure and porosity in research and practical applications.

The impact of chemical decomposition on weathering rock profiles formed on andesite has been evaluated in this study. Completely weathered rock forms through moderate

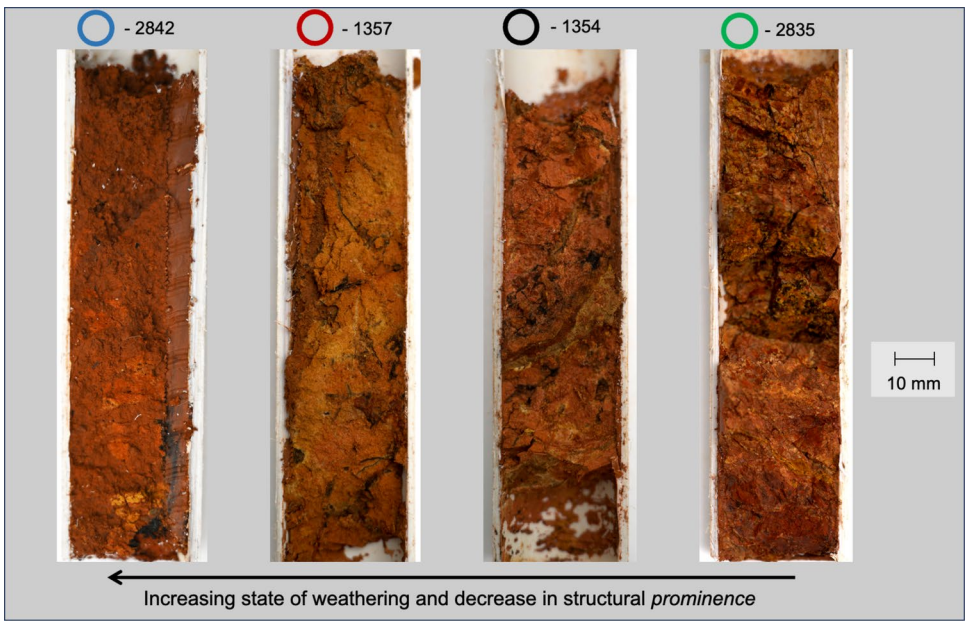

Fig. 18 Photographs taken of residual andesite sample 2842, completely weathered rock sample 1357 and 1354 retrieved near the residual soil and completely weathered rock interface and sample 2835 taken from the less weathered completely weathered rock (photographs taken by D Swart)

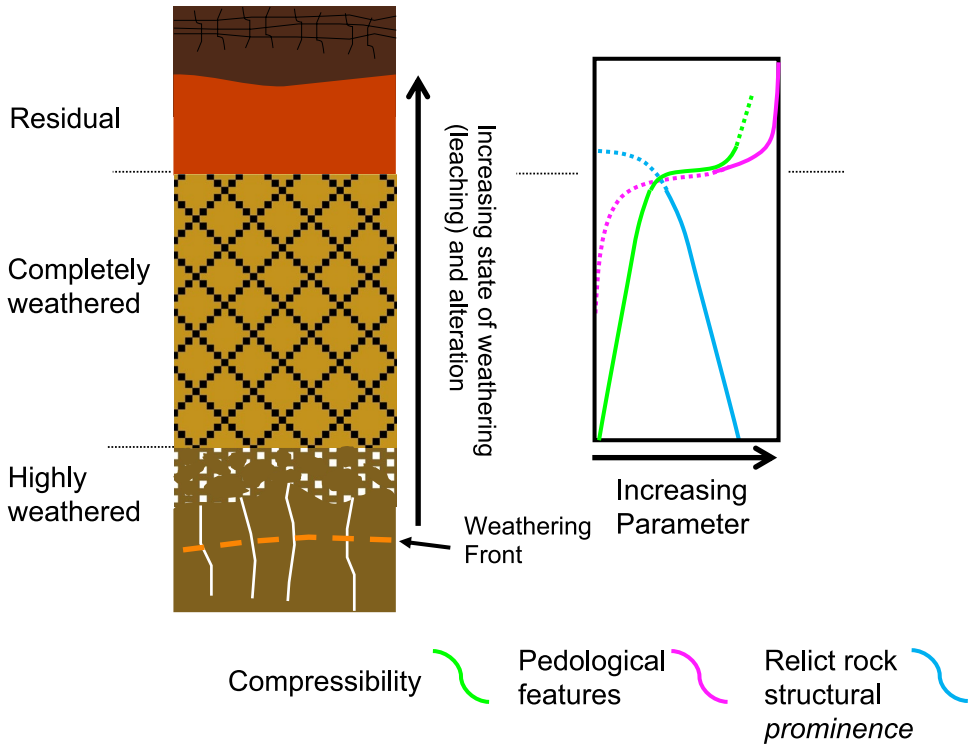

Fig. 19 Proposed generalised structural *prominence* and compressibility profile

to intense leaching of the parent rock to the point where most of the primary rock-forming minerals have been decomposed to various secondary minerals. The parent rock fabric and macro-structure, termed together as the relict rock structure, are mostly retained through the weathering process. The relict rock structure governs the porosity and pore geometry and has been known to provide stiffness and strength to the soil during compression. Volumetric strain does occur during weathering as minerals transform and change in both volume and shape which weaken and break bonds between mineral grains. This results in the material to be *soil-like* meaning it can be broken down into individual grains by hand. The broken-down grains typically behave as a low-plasticity silt which was the targeted material in this study. The weathering process forms a relatively porous material that has varying dry density and void ratio values depending on the parent rock and weathering environment.

The chemical composition of a weathering profile is predictable and follows a certain trend once the profile has been intensely weathered. The *soil-end* of a weathering profile is typically enriched in iron and aluminium through leaching away of more mobile elements such as calcium and sodium. These immobile ions form common clay minerals such as kaolinite and gibbsite.

A residual soil forms when the relict rock structure is lost through a combination of chemical and physical changes due to continued weathering. The structure of the residual soil is governed by pedological processes and, consequently, is more compressible. The resultant grading of residual soil is generally more clayey than the completely weathered rock and typically has a higher plasticity value.

The process through which completely weathered rock and residual soil forms is governed by the physical and chemical changes caused by chemical weathering. The degree of the weathering decreases with an increase in depth. The state of weathering can be quantified with the use of chemical weathering indices. *Structural prominence* is proposed as a single parameter to bridge the gap between visual, mechanical, and chemical assessments of weathering. It is suggested to provide better predictions of compressibility and stiffness than traditional parameters like void ratio or density. The structural *prominence* decreases as weathering increase and, consequently, this increases the compressibility of the material, regardless of the material's void ratio or dry density. The novel concept of structural *prominence* can be used to assist engineering geologists and geotechnical engineers to better understand the behaviour of completely weathered rock and residual soil. More studies using elaborate laboratory and field-based compression and shearing testing is recommended to assess the influence of structural prominence in weathering profiles.

Acknowledgements Thanks is extended to the Water Research Commission for the funding of project C2020-2021-00581 (*Natural and Anthropogenic Changes to the Subsurface Water Cycle and Ground Profile of the Vadose Zone in Developed Areas*) and project K5/2826

(*Vadose Zone Hydrology: Complexity and Anthropogenic Influences*, in print as *The Vadose Zone: From Theory to Practise*).

Funding Open access funding provided by University of Pretoria. This article was supported by Water Research Commission, C2020_2021-00581, Matthys Alois Dippenaar.

References

Al-Khafaji AWN, Andersland OB (1992) Equations for Compression Index Approximation. J Geotech Eng 118(1):148–153. https://doi.org/10.1061/(ASCE)0733-9410(1992)118:1(148)

ASTM D2487-17e1 (2020) Practice for Classification of Soils for Engineering Purposes (Unified Soil Classification System)'. ASTM International. https://doi.org/10.1520/D2487-17E01

Banerjee A, Chakrabarti R, Mandal S (2016) Geochemical anatomy of a spheroidally weathered diabase. Chem Geol 440:124–138. https://doi.org/10.1016/j.chemgeo.2016.07.008

Baveye P et al (2022) Lessons from a landmark 1991 article on soil structure: distinct precedence of non-destructive assessment and benefits of fresh perspectives in soil research. Soil Res 60:321. https://doi.org/10.1071/SR21268

Blight GE, Leong E-C (eds) (2012) Mechanics of residual soils, 2nd edn. CRC Press, Boca Raton

Blunt MJ (2001) Flow in porous media — pore-network models and multiphase flow. Curr Opin Coll Inter Sci 6(3):197–207. https://doi.org/10.1016/S1359-0294(01)00084-X

Bonnet M et al (2022) Weathering of Viamão granodiorite, South Brazil: Part 1 – Clay minerals formation and increase in total porosity. Geoderma 424:115968. https://doi.org/10.1016/j.geoderma.2022.115968

Bonnet M et al (2023) Weathering of Viamão granodiorite, south Brazil: Part 2 – Initial porosity of un-weathered rock controls porosity development in the critical zone. Geoderma 429:116247. https://doi.org/10.1016/j.geoderma.2022.116247

Bowen NL (1929) The Evolution of the Igneous Rocks. Nature 124(3126):474–475. https://doi.org/10.1038/124474a0

Brewer R (1965) Fabric and Mineral Analysis of Soils. Soil Sci 100(1):73

BS 1377–5 (1990) 'Methods of test for soils for civil engineering purposes. part 5: compressibility, permeability and durability tests'. BSI British Standards. Available at: 0-580-18030

Buttrick DB (1986) 'Wad and ferroan soil developed in the dolomitic area south of Pretoria'. Available at: https://repository.up.ac.za/handle/2263/82505 (Accessed: 10 November 2024)

Cho T, Ohta T (2022) A robust chemical weathering index for sediments containing authigenic and biogenic materials. Palaeogeogr Palaeoclimatol Palaeoecol 608:111288. https://doi.org/10.1016/j.palaeo.2022.111288

Clothier B (2008) 'Soil Pores', in Encyclopedia of Earth Sciences Series. Springer, pp 693–699 https://doi.org/10.1007/978-1-4020-3995-9_548

Cnudde V, Boone MN (2013) High-resolution X-ray computed tomography in geosciences: a review of the current technology and applications. Earth-Sci Rev 123:1–17. https://doi.org/10.1016/j.earscirev.2013.04.003

Daneshian B, Habibagahi G, Nikooee E (2021) Determination of unsaturated hydraulic conductivity of sandy soils: a new pore network approach. Acta Geotech 16(2):449–466. https://doi.org/10.1007/s11440-020-01088-3

Day PW (1981) Properties of Wad. Seminar on Engineering Geology of Dolomite Areas. University of Pretoria, Pretoria, pp 135–147

Dippenaar MA, Van Rooy JL, Davis G (2024) Engineering geological soil and rock description. Pretoria. South Africa: South African Institute for Engineering and Environmental Geologists (SAIEG). Available at: www.saieg.co.za

Dippenaar M (2014) Porosity reviewed: quantitative multi-disciplinary understanding, recent advances and applications in vadose zone hydrology. Geotech Geol Eng 32. https://doi.org/10.1007/s10706-013-9704-9

Dippenaar MA et al. (2022) The Vadose Zone: from theory to practise. Pretoria: Water Research Comission

Dos Santos JCBD et al (2018) Porosity and genesis of clay in gneiss saprolites: The relevance of saprolithology to whole regolith pedology. Geoderma 319:1–13. https://doi.org/10.1016/j.geoderma.2017.12.031

Dos Santos JCB, De Oliveira CS, Le Pera E et al (2022a) Saprolithology applied to pedology: Integrated study of soil and saprolite derived from crystalline rocks to better understand properties of whole regoliths along a climate gradient (NE Brazil). Geoderma 409:115602. https://doi.org/10.1016/j.geoderma.2021.115602

Dos Santos JCB, De Oliveira CS, Pera EL et al (2022b) Saprolithology applied to pedology: Mineral alteration in soil-saprolite profiles along a climate gradient in Triunfo Massif (NE Brazil). CATENA 213:106214. https://doi.org/10.1016/j.catena.2022.106214

Fedo CM, Wayne Nesbitt H, Young GM (1995) Unraveling the effects of potassium metasomatism in sedimentary rocks and paleosols, with implications for paleoweathering conditions and provenance. Geology 23(10):921. https://doi.org/10.1130/0091-7613(1995)023%3c0921:UTEOPM%3e2.3.CO;2

Fukue M, Okusa S (1987) Compression Law of Soils. Soils Foundations 27(1):23–34. https://doi.org/10.3208/sandf1972.27.23

Goldich SS (1938) A study in rock-weathering. J Geol 46(1):17–58. https://doi.org/10.1086/624619

Golparvar A, Kästner M, Thullner M (2021) Pore-scale modeling of microbial activity: What we have and what we need. Vadose Zone J 20(1):e20087. https://doi.org/10.1002/vzj2.20087

Hayes JL et al (2019) Porosity production in weathered rock: Where volumetric strain dominates over chemical mass loss. Sci Adv 5(9):eaao0834. https://doi.org/10.1126/sciadv.aao0834

Helliwell JR et al (2013) Applications of X -ray computed tomography for examining biophysical interactions and structural development in soil systems: a review. Euro J Soil Sci 64(3):279–297. https://doi.org/10.1111/ejss.12028

Hencher S (2024) Practical Engineering Geology. 2nd edn. London: CRC Press. https://doi.org/10.1201/9781003348894

Hu W et al (2023) Soil structural vulnerability: Critical review and conceptual development. Geoderma 430:116346. https://doi.org/10.1016/j.geoderma.2023.116346

Huda W, Abrahams RB (2016) Review of radiologic physics, 4th edn. Lippincott Williams & Wilkins, Philadelphia

ISRM IS for RM (1981) 'Suggested Methods for the Rock Characterization, Testing and Monitoring', in ISRM Commission on Testing Methods. Oxford: Pergamon Press

Jaques DS et al (2020) Changes in the physical, mineralogical and geomechanical properties of a granitic rock from weathering zones in a tropical climate. Rock Mech Rock Eng 53(12):5345–5370. https://doi.org/10.1007/s00603-020-02240-x

Jaques DS et al (2021) Morphological and mineralogical characterization of weathering zones in tropical climates: a basis for understanding the weathering process on granitic rocks in southeastern Brazil. J South Am Earth Sci 108:103187. https://doi.org/10.1016/j.jsames.2021.103187

Kellogg CE (1930) Preliminary study of the profiles of the principal soil types of Wisconsin. Madison: Published by the state (Bulletin / Wisconsin Geological and natural history survey ; no. 77A). Available at: https://catalog.hathitrust.org/Record/100223373 (Accessed: 10 November 2024)

Knappett J, Craig RF, Craig RF (2012) *Craig's soil mechanics*. 8th ed. Abingdon, Oxon ; New York: Spon Press

Lenhardt N, Eriksson PG (2012) 'Volcanism of the Palaeoproterozoic Bushveld Large Igneous Province: The Rooiberg Group Kaapvaal Craton, South Africa. Precambrian Res 214215:82–94. https://doi.org/10.1016/j.precamres.2011.12.003

Letey J (1991) The study of soil structure - Science or art. Soil Res 29(6):699. https://doi.org/10.1071/SR9910699

Li ZS, Tang LS (2019) Using synchrotron-based x-ray microcomputed tomography to characterize water distribution in compacted soils. Adv Mater Sci Eng 2019(1):7147283. https://doi.org/10.1155/2019/7147283

Liu X et al (2022) Chemical weathering indices and how they relate to the mechanical parameters of granite regolith from southern China. CATENA 216:106400. https://doi.org/10.1016/j.catena.2022.106400

Makhubela TV et al (2021) 'Erosion rates and weathering timescales in the eastern Great Escarpment South Africa. Chem Geol 580:120368. https://doi.org/10.1016/j.chemgeo.2021.120368

Mees F et al (2003) Applications of X-ray computed tomography in the geosciences. Geol Soc London, Special Public 215(1):1–6. https://doi.org/10.1144/GSL.SP.2003.215.01.01

Meunier A et al (2013) The weathering intensity scale (WIS): An alternative approach of the Chemical Index of Alteration (CIA). Am J Sci 313:113. https://doi.org/10.2475/02.2013.03

Mitchell JK, Soga K (2005) Fundamentals of soil behavior, 3rd edn. John Wiley & Sons, Hoboken, N.J

National Research (2001) Basic Research Opportunities in Earth Science. Washington, D.C.: National Academies Press https://doi.org/10.17226/9981

Nesbitt HW, Young GM (1982) Early Proterozoic climates and plate motions inferred from major element chemistry of lutites. Nature 299(5885):715–717. https://doi.org/10.1038/299715a0

Obermeier SF, Langer WH (1986) 'Relationships between geology and engineering characteristics of soils and weathered rocks of Fairfax County and vicinity, Virginia', Professional Paper [Preprint]. https://doi.org/10.3133/pp1344

Phillips JD, Pawlik Ł, Šamonil P (2019) Weathering fronts. Earth-Sci Rev 198:102925. https://doi.org/10.1016/j.earscirev.2019.102925

Rabot E et al (2018) Soil structure as an indicator of soil functions: A review. Geoderma 314:122–137. https://doi.org/10.1016/j.geoderma.2017.11.009

Riebe C et al (2021) Anisovolumetric weathering in granitic saprolite controlled by climate and erosion rate. Geology 49:551. https://doi.org/10.1130/G48191.1

Rietveld HM (1969) A profile refinement method for nuclear and magnetic structures. J Appl Crystallogr 2(2):65–71. https://doi.org/10.1107/S0021889869006558

Rocchi I, Coop MR, Maccarini M (2017) The effects of weathering on the physical and mechanical properties of igneous and metamorphic saprolites. Eng Geol 231:56–67. https://doi.org/10.1016/j.enggeo.2017.10.003

Saha S et al (2024) Impact of remolded soil fabric on the volumetric deformation behavior of clayey soils. Trans Geotech 44:101158. https://doi.org/10.1016/j.trgeo.2023.101158

SANS 3001-GR1 (2013) Civil engineering test methods. Part GR1: Wet preparation and particle size analysis. Edition 1.2. Pretoria: South African Bureau of Standards (SABS)

SANS 3001-GR10 (2013) Civil engineering test methods. Part GR10: Determination of the one-point liquid limit, plastic limit, plasticity index and linear shrinkage. Pretoria: South African Bureau of Standards (SABS)

Schweitzer JK, Hatton C, de Waal S (1995) Regional lithochemical stratigraphy of the Rooiberg Group, upper Transvaal Supergroup: a proposed new subdivision. S Afr J Geol 98:245–255

Sergeev N (2023) Quantifying weathering intensity using chemical proxies: a weathering index AFB. Aust J Earth Sci 70(2):260–284. https://doi.org/10.1080/08120099.2023.2137585

Silva LFVD et al (2022) Saprolite: A bibliometric study from 1990 to 2020. J South Am Earth Sci 115:103729. https://doi.org/10.1016/j.jsames.2022.103729

Sturrock CJ (2022) 'Optimising the Scanning Process: Demystifying the Dark Art of Optimising Microtomography Scan Settings', in S. Jon Mooney et al. (eds) X-ray Imaging of the Soil Porous Architecture. Cham: Springer International Publishing, pp. 39–55. https://doi.org/10.1007/978-3-031-12176-0_4

Summerfield MA (2014) Global Geomorphology. 1st edn. Routledge. Available at: https://www.perlego.com/book/1557141/global-geomorphology-pdf?utm_source=google&utm_medium=cpc&campaignid=15853719261&adgroupid=166297292553&gad_source=1&gclid=Cj0KCQiA0MG5BhD1ARIsAEcZtwQ3cc3XeNi9ToNKB62Z4A3_k8CaGKbMdKixKu8RFnFIaWiKU7CFvUQaAu7wEALw_wcB (Accessed: 10 November 2024)

Swart D, Dippenaar MA, Van Rooy JL (2019) Mechanical and hydraulic properties of residual dolomite and wad. South Afr J Geol 122(3):379–388. https://doi.org/10.25131/sajg.122.0024

Swart D, Dippenaar MA, Van Rooy JL (2023) Field tests for the identification of silts. Bull Eng Geol Environ 82(11):425. https://doi.org/10.1007/s10064-023-03442-7

Terribile F *et al.* (2022) 'Soil sampling and preparation for X-ray Imaging', in S. Jon Mooney et al. (eds) X-ray imaging of the soil porous architecture. Cham: Springer International Publishing, pp. 19–38 https://doi.org/10.1007/978-3-031-12176-0_3

Terzaghi K (1943) Theoretical soil mechanics. 1st edn. Wiley. https://doi.org/10.1002/9780470172766

Townsend FC, Manke PG, Parcher JV (1969) 'Effects of remolding on the properties of a lateritic soil', Highway Res Rec [Preprint], (284). Available at: https://trid.trb.org/View/121427 (Accessed: 9 November 2024)

Van der Merwe DH (1964) The weathering of some basic igneous rocks and their engineering properties. Civil Eng Siviele Ingenieurswese 1964(12):213–222. https://doi.org/10.10520/AJA10212019_17003

Van Tol J (2020) Hydropedology in South Africa: Advances applications and research opportunities. South Afr J Plant Soil 37(1):23–33. https://doi.org/10.1080/02571862.2019.1640300

Vogel H et al (2022) A holistic perspective on soil architecture is needed as a key to soil functions. Eur J Soil Sci 73(1):e13152. https://doi.org/10.1111/ejss.13152

Wang N, Zhang Z (2024) Soil pore structure and its research methods: A review. Soil Water Res 19(1):1–24. https://doi.org/10.17221/64/2023-SWR

Wang Y, Rahman SS (2023) Numerical modelling of reservoir at pore scale: A comprehensive review. J Comput Phys 472:111680. https://doi.org/10.1016/j.jcp.2022.111680

Wang Y et al (2024) Study on the mechanical properties and microscopic evolution mechanisms of weathered granite soil. Sci Rep 14(1):24388. https://doi.org/10.1038/s41598-024-75092-y

Weinert H (1980) Natural road construction materials of Southern Africa. Available at: http://hdl.handle.net/10204/3840

Wesley LD (1990) Influence of Structure and Composition on Residual Soils. J Geotech Eng 116(4):589–603. https://doi.org/10.1061/(ASCE)0733-9410(1990)116:4(589)

Wesley LD (2010) Geotechnical Engineering in Residual Soils. 1st edn. Wiley. https://doi.org/10.1002/9780470943113

Wesley LD (2019) 'Genuine and false pre-consolidation and yield pressures', E3S Web of Conferences. Edited by A. Tarantino and E. Ibraim, 92, p 05001. https://doi.org/10.1051/e3sconf/201992205001

Wildenschild D, Sheppard AP (2013) X-ray imaging and analysis techniques for quantifying pore-scale structure and processes in subsurface porous medium systems. Adv Water Resour 51:217–246. https://doi.org/10.1016/j.advwatres.2012.07.018

Wilson MJ (2004) 'Weathering of the primary rock-forming minerals: processes, products and rates. Clay Minerals. 2018/07/09 Edn 39(3):233–266. https://doi.org/10.1180/0009855043930133

Wu H, Zhang Z, Dias D (2024) 'Prediction on compression indicators of clay soils using XGBoost with Bayesian optimization', J Central South Univ. https://doi.org/10.1007/s11771-024-5681-9.

Yong RN, Nakano M, Pusch R (2012) Environmental Soil Properties and Behaviour. CRC Press. https://doi.org/10.1201/b11658